

Response to Referee #1

We are grateful to the reviewer for their time and energy in providing helpful comments and guidance that have improved the manuscript. In this document, we describe how we have addressed the reviewer's comments. Referee comments are shown in italics and author responses are shown in regular text.

This paper describes a new model for terrestrial biosphere processes that can be run in offline mode and coupled to an atmospheric chemistry-climate model. Aside from the model description, the authors show substantial validation of the model (YIBs) in three different configurations. The model performs well compared to the observations presented and to other more established terrestrial biosphere models. Compared to other models it also has a fairly mature treatment of ozone damage and BVOC emissions. This represents a substantial contribution to the earth system science community, as evidenced by the fact that YIBs has already been used in previously published work. The paper is well structured and well written, and the abstract is clear and concise. It is appropriate for GMD and I recommend it for publication in this journal. However I do have recommendations as outlined below.

→ Thank you for the positive evaluation of this study and support of the YIBs model.

1. Model spin up: Why are different periods used for each of the experiments? In the supplement, it is stated that 80 years was long enough to get a net land sink of 2 PgC yr^{-1} . Was this initial condition only used for the global offline simulations? Why was only 60 years used for the online simulations?

For the site simulations, 30 years is a very short spin-up period, and it's likely that the respiration fluxes are still a function of the initial soil carbon. A longer spin-up would affect both the annual total and seasonal cycles of ecosystem respiration, and would therefore alter the NEE results. Since it is unknown to what level the soil carbon is in equilibrium at each site, I recommend removing the discussion of site simulated NEE. It could warrant a whole paper on its own, but as it stands this does not substantially add to the paper.

→ We confirm and verify that all 3 experimental configurations (site level, YIBs-offline and YIBs-online) use derived soil carbon pools from a $60+80=140$ year spin-up as the initial conditions. The 140-year soil carbon pool spin-up period is performed with YIBs-offline for recycling year 1980 forcings (year 2000 for YIBs-online initial soil carbon pools). Site-level and global on-line simulations involve additional 30-year spin-ups.

YIBs requires minimum hourly resolution meteorological input data, which is only available from 1980. Hence, we do not adopt preindustrial (e.g. 1750 or 1850) conditions as the base period for the spin-up.

We completely re-wrote the Supplementary Information to give a much more transparent and lucid description of the soil carbon spin-up process:

“Soil carbon pool spin-up process using YIBs-offline

Studies investigating terrestrial carbon fluxes usually initialize models for the preindustrial period when human perturbations are negligible and soil carbon pools are considered to be at an equilibrium state (Huntzinger et al., 2013; Sitch et al., 2015). YIBs requires (minimum) hourly meteorological input data fields, which are only available from 1980. Therefore, to spin-up YIBs, we adapt the approach of Wutzler and Reichstein (2007), who applied a transient correction to the soil carbon pools so that the simulated stocks match observations.

We apply YIBs-offline to spin-up the soil carbon pools that provide the initial conditions for all 3 experimental configurations (site-level, YIBs-offline and YIBs-online). The spin-up process proceeds in 2 stages. In the first stage, we set a uniform initial height H_0 for each PFT (Table 1) and run YIBs-offline for 60 years using fixed CO₂ concentrations and meteorological forcings for the year 1980 to allow vegetation carbon to equilibrate. By the end of the first stage spin-up run, the year-to-year variations of global average tree height, LAI, GPP, and NPP are all within $\pm 0.05\%$. In the second stage, the derived equilibrium tree heights from the first stage and the global soil carbon content at the top 30 centimeters (Batjes (2009) provide the initial conditions for an 80-year run (again using fixed CO₂ concentrations and meteorological forcings for the year 1980) until the transient NEE is equal to -2 Pg C a^{-1} , a value supported by observations and multi-model ensembles (Piao et al., 2013).

Following this 2 stage 60+80=140 year total spin-up, the derived soil carbon pools represent the state for the year 1980. For YIBs site level simulations: the derived spun-up soil carbon pools for 1980 are used as initial conditions. For YIBs-offline simulations: the derived spun-up soil carbon pools and equilibrium tree heights for 1980 are used as initial conditions for the 1980-2011 transient period. For the on-line simulations with NASA ModelE2-YIBs: the entire 140-year process described above is repeated with fixed WFDEI meteorology and atmospheric CO₂ conditions for the year 2000 values. The derived spun-up soil carbon pools and equilibrium tree heights for 2000 are used as initial conditions for the present-day climatological coupled global carbon-chemistry-climate simulation.”

We further clarified the spin-up procedure and extensions for each configuration in the main manuscript text:

4.1 Site-level simulations (Lines 557-562):

“The soil carbon pool initial conditions at each site are provided by the 140-year spin up procedure using YIBs-offline (Supplement). An additional 30-year spin up is conducted for each site-level simulation using the initial height H_0 for corresponding PFT (Table 1) and the fixed meteorology and CO₂ conditions at the first year of observations. Then, the simulation is continued with year-to-year forcings at the specific site for the rest of measurement period.”

4.2 Global off-line simulation (YIBs-offline) (Lines 572-573):

“The soil carbon pool and tree height initial conditions are provided by the 140-year spin up procedure using YIBs-offline (Supplement).”

4.3 Global on-line simulation in NASA ModelE2-YIBs (Lines 591-595):

“In NASA ModelE2-YIBs, initial conditions for soil carbon pools and tree heights are provided by the 140-year spin-up process described in the Supplement using YIBs-offline but for year 2000 (not 1980) fixed WFDEI meteorology and atmospheric CO₂ conditions. The NASA ModelE2-YIBs global carbon-chemistry-climate model is run for an additional 30 model years.”

Since the site-level simulations use soil carbon pools from 140-year total spin-up as initial conditions for 1980, and then an additional 30 years spin-up for each individual site, we would like to retain the discussion of site-level simulated NEE. Our main reason is that NEE is the directly measured quantity whereas GPP is derived from the directly measured NEE. However, we do certainly agree with the referee that NEE is sufficiently complex, sensitive and critical to warrant an entire study in its own right.

2. GPP: Please state where the GPP data comes from: was it downloaded from a website? Processed by the authors from NEE? Also, there is uncertainty associated with the flux tower GPP, as it is calculated from the measured NEE, which is itself uncertain (e.g. Papale et al. 2006, or see biome-dependent uncertainty estimates in Luyssaert et al. 2007, both attached). It would be useful to know the ability of the model in light of the uncertainty. For example, in Figure 4: a relative bias of 50% in GPP would be very high if the uncertainty in the GPP is around 20%. It would be useful to include uncertainty in the Flux Tower analysis – for example, the standard deviation of measured GPP could be used as a proxy for uncertainty in the flux, or general guidelines for biome-level uncertainty in Luyssaert et al. 2006.

→ In the section 2.1 (Lines 132-135), we state the origins of the GPP data:

“To validate the YIBs model, we use eddy covariance measurements from 145 flux tower sites (Fig. 1), which are collected by the North American Carbon Program (Schaefer et al., 2012) (K. Schaefer, personal communication) and downloaded from the FLUXNET (<http://fluxnet.ornl.gov>) network.

The error bars in Figs. S2 and S3 show that derived FLUXNET GPP uncertainties in terms of standard deviation of the interannual variations are small for most sites without crop rotation. We agree that intraspecific uncertainties could be large. As a result, we check the intraspecific variations in GPP and NEE and present results in Table S2 (we put in SI because the paper is already lengthy). We add the following statement (Lines 644-649)

“YIBs model performs simulations at the PFT level while measurements show large uncertainties in the carbon fluxes among biomes/species within the same PFT (Luyssaert et al., 2007). The simulated intraspecific variations (in the form of standard deviation) are smaller than the measured/derived values for most PFTs (Table S2), likely because of the application of fixed photosynthetic parameters for each PFT (Table 1).”

3. Judging from Table 1, the tundra PFT is most like a shrub but with reduced productivity. Does phenology apply to the tundra PFT?

→ Yes. We clarified in the revised text: (Lines 325-327):

“The shrub phenology applies for shrubland in tropical and subtropical areas, as well as tundra at the subarctic regions, though the phenology of the latter is usually dependent on temperature alone because the climatological soil temperature is <12 °C.”

4. Model description: A few questions about the model formulation:

- In Equation 19, $(1-\lambda)NPP$ is allocated toward the different vegetation carbon pools.

What happens to the rest of the carbon assimilated through NPP (λNPP)?

- Nitrogen in wood: From equation 23c, it looks like all wood respire. Is it accurate to assume that all wood respire? In TRIFFID there is an additional parameter for calculating N in stems that approximates the respiring stemwood based on height (e.g. Friend et al. 2003).

- Is this model available for people to use? Is there a website?

→ (1) The rest of carbon is not used for carbon allocation in the current version, but is included in the litterfall for soil respiration. We adopted the carbon allocation scheme from TRIFFID, which also simulates dynamic changes in vegetation fraction. The portion of NPP (λNPP) is used for the spreading but is turned off in the current YIBs version. In future, we expect to extend the YIBs model to a fully dynamic vegetation model with additional treatment of fractional changes. We clarify (Lines 433-434):

“In the current model version, we turn off the fractional changes by omitting λNPP in the carbon allocation but feeding it as input for the soil respiration.”

(2) We rechecked and found that the original function 23c was not presented correctly as reported in Cox (2001) and in the YIBs code. Yes, both TRIFFID and YIBs calculate N of stem based on tree height and LAI. We revised equation 23c correctly: $N_w = n_{wl} \cdot n_0 \cdot \eta \cdot H \cdot LAI$. We show the values of η in Table 1.

(3) We have added a new section “Code availability” (Lines 799-804):

“The YIBs model (version 1.0) site-level source code is available at https://github.com/YIBS01/YIBS_site. The source codes for the global off-line and

global on-line versions of the YIBs model (version 1.0) are available through collaboration. Please submit request to X. Yue (xu.yue@yale.edu) and N. Unger (nadine.unger@yale.edu). Auxiliary forcing data and related input files must be obtained independently.”

5. As explained in Section 5.1, there is a high correlation between modelled and observed GPP at the ENF sites. Is this definitely due to the frost hardening? Was the correlation evaluated with and without frost hardening? There are many other temperature dependencies in the photosynthesis equations so it seems possible that other factors are affecting the GPP in winter.

→ We performed additional sensitivity tests that turned off the frost hardening for ENF. Simulated GPP without frost hardening on average correlates with observations by 0.81, very slightly lower than the value of 0.84 with frost hardening over the 54 ENF sites. In winter (December-January-February), the average modeling bias is $-0.20 \text{ g C m}^{-2} \text{ day}^{-1}$ (-15%) with frost hardening and $0.50 \text{ g C m}^{-2} \text{ day}^{-1}$ (38%) without. We do agree that other factors may also contribute to the modeling biases. We revise the statement (Lines 619-620):

“The correlation is also high for ENF sites even though phenology is set to a constant value of 1.0.”

6. Table 3 and related text in Section 5.2: This section of text is difficult to follow, mainly because the text explains carbon fluxes for large regions (ie: All tropics) in terms of % of the global total, while the table shows actual fluxes for smaller regions – this makes it cumbersome to cross-reference the table. One suggestion is to add columns for All Tropics and All Temperate regions.

Also, is 46% meant to refer to both the NPP and Rh?

The final sentence about the NEE differences between the tropical and temperate biomes needs some further evidence or explanation: If the warmer biomes have a higher dark respiration, this implies that they also have higher V_{cmax} and possibly GPP, which would contribute to a more negative NEE in the tropics (unless tropical GPP is limited by radiation, J_e , which in some regions is likely the case – in this case higher V_{cmax} would result in increased R_{dc} but not higher GPP). Was dark respiration output by the model?

→ We have added one column for tropics as suggested. In the original manuscript, we were summing up values in the Amazon, Central Africa and Indonesia as the “tropics” definition. We revise the tropics definition to encompass the latitude belt (23°S-23°N). Values for temperate regions are very close to (global - tropics) and are not included. Using this revised “tropics” definition, both NPP and Rh account for 57% of the global total.

Yes. We agree that our explanation for NEE differences was not clear. In the revised text, we have deleted the original explanation to avoid confusion. NEE is the net difference between 2 large and similar quantities: Rh and NPP, making NEE highly sensitive to even small uncertainties in Rh and NPP and therefore to many propagating factors (e.g. temperature, PAR differences). For example, in our calculation, tropical Rh accounts for 57.3% of global total and NPP accounts for 56.6%.

7. *Figure 6: It would help to have a legend showing the color-coding for the seasons.*

→ We have added color indicators at the bottom of Fig. 6.

8. *Conclusions and discussion: I disagree with the statement that “The vegetation parameters, V_{cmax25} , m , and b are not well calibrated for the tropical forest rainforest biome due to the limited availability of tropical site measurement data (Fig. 1).” While it is true that relative to other biomes, there is a lack of data for tropical forest biomes, this is not what is shown in Figure 1. This figure shows there is only 1 flux tower used in this study (not the authors fault, there is a lack of flux towers in the Tropics especially ones with enough data to calculate GPP from the NEE). However, there is a fair amount of data which could be used to calculate photosynthesis parameters in the Tropics, see for example Figure 2 in Kattge et al. 2011.*

→ We agree with the referee, and the original statement as written was incorrect. We change the sentence to emphasize the point we intended to make: “The vegetation parameters, $V_{cmax\ 25}$, m , and b (Table 1), are fixed at the PFT level, which may induce uncertainties in the simulation of carbon fluxes due to intraspecific variations (Kattge et al., 2011)”. (Lines 772-774)

9. *Why was the MTE from Jung et al. 2009 used, instead of the MTE described in the 2011 paper? The 2009 product was made to reproduce a model (LPJmL), using fPAR simulated in LPJmL.*

For clarity, we add the statement (Lines 155-156):

“This product was made to reproduce a model (LPJmL) using the fraction of absorbed PAR simulated in LPJmL.”

We do not consider this choice a shortcoming because (i) most of the satellite products used in the validation necessarily involve a model at some stage in the processing; and (ii) Figure 7 shows that the two Jung et al. MTE GPP products used for large-scale GPP evaluation differ by only $\sim 15 \text{ Pg a}^{-1}$, much smaller than the spread in the model inter-comparison.

10. Technical comments: Abstract: An opinion: I'm not sure if the word "inextricably" is the best choice for beginning a paper attempting to explain these connections. Perhaps "intricately" is a better word?

→ We agree and changed to "intricately" following the referee's suggestion.

11. Dark respiration is referred to as R_d in equation 5 and R_{dc} in Equation 22.

→ The symbol R_{dc} has been changed to R_d in the revised text.

12. Page 3164, Line 20: remove "vs. higher"

→ Corrected.

Response to Referee #2

We are grateful to the reviewer for their time and energy in providing helpful comments and guidance that have improved the manuscript. In this document, we describe how we have addressed the reviewer's comments. Referee comments are shown in italics and author responses are shown in regular text.

This manuscript presents a new land surface model to be coupled with the NASA Model E2. The model is a combination of previous land surface schemes and functional modules – TRIFFID, CASA, Biome-BGC, MEGAN, and the ozone damage scheme employed by Sitch et al (2007). The paper is generally well written, though often a little dense. The research represents a great deal of work, model development and evaluation are substantial research efforts, especially for such a small research team. However, this research would benefit from well developed objectives and strong arguments for the model units that were chosen to form the basis of the model.

→ We appreciate the reviewer's positive evaluation and recognition of the hard work (8-years combined total by the co-authors). We have revised the paper accordingly to strengthen the objectives and explanations for the choice of the model components as detailed below.

It appears that the goal of this research was to develop a state of the art LSM that terrestrial ecosystem processes that are important for interactions with atmospheric chemistry, e.g. BVOC emissions, O₃ damage to plants, etc. Though this objective is never clearly stated. Without a clearly stated objective the need for another LSM cannot be justified and the choice of how to represent processes within the model are apparently ad hoc. Why not use a complete, state-of-the-art LSM that represents the most processes relevant to your purpose and then include a state of the art BVOC and O₃ model. For example, the authors acknowledge their model does not represent N and P cycling. This could have been achieved by collaborating with CABLE, CLM, or JSBACH modelling groups. Furthermore, in my limited understanding of land ecosystem – atmospheric chemistry interactions, gaseous N species are essential to many reactions and so an N cycle would be essential to accurate coupling of terrestrial ecosystems with atmospheric chemistry. Other state-of-the-art LSMs which represent an N cycle such as LM3 or O-CN could have formed the basis of this model. It is as if this model has been developed in isolation from the land surface and terrestrial biosphere modelling community, and the many advances in process representation from that community over the last decade.

The decision making process about which parts from which model to include is not at all discussed and seems ad hoc, there is no evaluation of competing alternative schemes. So much has been learnt over the past decade about LSMs and how to improve them, for example Zaehle et al (2014) is cited but no information from that detailed model evaluation is used to inform the development of this new model. The model purpose, and therefore the criteria to assess how to build the model are not apparent. This research needs, and would really benefit from a clear statement of purpose which would then

provide a decision criteria for how constructing the YIBs model.

(1) YIBs objective

The reviewer is correct that the objective of YIBs is to provide a fully coupled framework to study carbon-chemistry-climate interactions; a dynamic land carbon cycle component integrated within a global chemistry-climate model. Atmospheric chemistry means reactive radiatively-active species, ozone and aerosols, not the long-lived greenhouse gases CO₂ and N₂O that do not react in the troposphere. The introduction section second paragraph is already devoted to a detailed discussion of the few carbon-chemistry studies available in the published literature, and ends with “These coupled interactions are often not adequately represented in current generation land biosphere models or global chemistry-climate models.” We strengthen the case by adding to the end of the paragraph (Lines 76-84):

“Global land carbon cycle models often prescribe off-line ozone and aerosol fields (e.g., Sitch et al., 2007; Mercado et al., 2009), and global chemistry-climate models often prescribe fixed off-line vegetation fields (e.g., Lamarque et al., 2013; Shindell et al., 2013a). However, multiple mutual feedbacks occur between vegetation physiology and reactive atmospheric chemical composition that are completely neglected using these previous off-line approaches. Model frameworks are needed that fully 2-way couple the land carbon cycle and atmospheric chemistry, and simulate the consequences for climate change.”

The study objective is now clearly stated in the first sentence of the next paragraph (Lines 86-88):

“Our objective is to present the description and present-day evaluation of the Yale Interactive terrestrial Biosphere Model (YIBs) version 1.0 that has been developed for the investigation of carbon-chemistry-climate interactions.”

We add to the first sentence of the abstract (Lines 11-13):

“The land biosphere, atmospheric chemistry and climate are intricately interconnected yet the modeling of carbon-climate and chemistry-climate interactions have evolved as entirely separate research communities.”

We add to the Introduction third paragraph (Lines 95-97):

“To our knowledge, this study represents the first description and validation of an interactive climate-sensitive closed land carbon cycle in NASA ModelE2.”

In addition to the focus on carbon-chemistry-climate interactions, we assert that YIBs is justified because YIBs outperforms many existing “state of the art” land carbon cycle models as demonstrated in: Yue and Unger, Ozone vegetation damage effects on gross primary productivity in the United States, ACP, 14, 9137-9153, 2014; in this work (e.g.

Figure 7); and pointed out by Referee #1. Given the poor performance status of GPP simulations in existing land models (e.g., Schaefer et al., 2012) and the large uncertainties in future land carbon cycle model responses (Friedlingstein et al., 2006; Friedlingstein et al., 2014), we argue that there is, in fact, an urgent need for fresh interdisciplinary perspectives.

(2) Choice of model components in YIBs and development strategy

The reviewer raises some interesting questions pertinent to interdisciplinary Earth system science research. It was an option that we could have taken an existing land carbon cycle model, added BVOC emissions and ozone damage and coupled that to NASA ModelE2 global chemistry-climate model. Indeed, at the start of the project, we actively discussed use of an existing community land model. The top candidates were JULES, CLM or LPJ because of our on-going relationships with these groups. We do run JULES and CLM on our local supercomputer already and we were given access to LPJ code several years ago. In the end, we decided to adopt a less conventional strategy and build up YIBs step by step for several reasons including: (i) The major advantage of our strategy is that we know first-hand the intimate details of the scientific processes included in YIBs, because we coded it ourselves over a period of 5 years. We assert that this intimate interdisciplinary knowledge offers potentially deeper insights and a greater possibility for advances in carbon-chemistry interactions research than taking an existing land model as a “black box”; (ii) A technical concern was that we needed to have 30-minute or maximum 1-hour integration time-step for full coupling to the atmospheric chemistry (to simulate the strong diurnal cycles important in the chemistry). Many land carbon cycle models use longer integration time-steps (e.g. minimum daily) as their default because they incorporate dynamical climate-sensitive PFT distributions and because their main applications are longer-term (decadal, century scales) evolution of atmospheric CO₂. The time-step is described up front in the abstract because of its central importance to carbon-chemistry coupling “Off-line YIBs has hourly and on-line YIBs has half-hourly temporal resolution.”; (iii) A budget concern at the start of the project was that we did not have resources for a multi-institute collaboration. Our approach was the much less expensive option, with successful results because YIBs outperforms many existing models.

YIBs has been developed step-by-step with solid decision-making at each stage choosing the most appropriate sub-component for our purpose. Co-author Unger has > 13 years experience documented in > 40 publications with NASA ModelE/ModelE2 global chemistry-climate model and therefore the model’s land surface scheme. Until now, the NASA ModelE2 land surface sub-model did not incorporate an interactive climate-sensitive closed land carbon cycle model and the atmospheric chemistry “saw” a different prescribed vegetation cover than the climate model’s internal scheme (Section 3.7 Lines 531-533: “the default NASA ModelE2 computes dry deposition using fixed LAI and vegetation cover fields from Olson et al. (2001), which are different from the climate model’s vegetation scheme (Shindell et al., 2013b).”).

We have replaced the original Introduction paragraph: “Previously, we presented and evaluated an off-line regional version of YIBs that was applied to assess ozone damage

effects on GPP in the U.S. (Yue and Unger, 2014); and an on-line global version of YIBs that was used to investigate BVOC-chemistry-climate interactions (Unger, 2013; Unger et al., 2013a; Unger, 2014a, b; Unger and Yue, 2014). Here, we describe the recent updated functionalities of the YIBs model that now represents the complete land carbon cycle: interactive carbon assimilation, allocation, autotrophic and heterotrophic respiration, and dynamic tree growth (changes in both height and LAI). The model also implements updated phenology schemes developed based on the inter-comparison of 13 phenological models (Yue et al., 2015).”

with a new clearer section:

“1.1 YIBs design strategy

Many land carbon cycle models already exist (e.g. Sitch et al., 2015 and references therein; Schaefer et al., 2012 and references therein). We elected to build YIBs in a step-by-step process such that our research group has intimate familiarity with the underlying scientific processes, rather than adopting an existing model as a “black box”. This unconventional interdisciplinary approach is important for discerning the complex mutual feedbacks between atmospheric chemistry and the land carbon sink under global change. The development of YIBs land carbon cycle model has proceeded in three main steps. The first step was the implementation of vegetation biophysics, photosynthesis-dependent BVOC emissions and ozone vegetation damage that have been extensively documented, validated and applied in 7 previous publications (Unger, 2013; Unger et al., 2013b; Unger, 2014a, b; Unger and Yue, 2014; Yue and Unger, 2014; Zheng et al., 2015). The second step was the selection of the YIBs default phenology scheme based on rigorous inter-comparison of 13 published phenological models (Yue et al., 2015). This study represents the third step to simulate the closed climate-sensitive land carbon cycle: implementation of interactive carbon assimilation, allocation, autotrophic and heterotrophic respiration, and dynamic tree growth (changes in both height and LAI). For this third step, we purposefully select the mature, well-supported, well-established, readily available and accessible community algorithms: TRIFFID (Cox, 2001; Clark et al., 2011) and the Carnegie-Ames-Stanford Approach (CASA) (Potter et al., 1993; Schaefer et al., 2008). TRIFFID has demonstrated previous usage in carbon-chemistry-climate interactions research.”

YIBs has been developed in close connection with the land carbon cycle modeling community. The phenology sub-model was developed in collaboration with leading internationally-renowned phenology and carbon cycle experts (Yue, X., N. Unger, T.F. Keenan, X. Zhang, and C.S. Vogel, [Probing the past 30 year phenology trend of US deciduous forests](#), *Biogeosciences Discuss.*, 12, 6037-6080, doi:10.5194/bgd-12-6037-2015, 2015). We have an on-going relationship with the JULES community development team who are always encouraging and responsive to our group. Co-author Unger spent sabbatical with the JULES development team in the UK. One could make a strong case that implementing TRIFFID into a different host global climate model (other than the Hadley Center models e.g. HadGEM2/3) is in of itself a worthy scientific endeavor. We eagerly anticipate that YIBs will participate in future multi-model inter-comparison projects focused on the land carbon cycle. YIBs results have been and will continue to be

submitted for presentation at land carbon cycle and chemistry-climate conferences and meetings. As such, YIBs is becoming well integrated into the land modeling community. Finally, in making the code publically available (Code Availability Section), we anticipate expanding the user base beyond our group and thereby facilitating new developments.

(3) C-N coupling

We agree with the reviewer that N and P cycles are important processes for the terrestrial C cycle. The coupled C-N was not an initial priority for YIBs because of the massive uncertainties in the current models, for instance in sign of response. In the future, with adequate resources and personnel, we do plan to include N and P cycles in NASA ModelE2-YIBs. For example, we are especially curious about P in the Amazon (e.g., Mercado et al., 2011). To our knowledge, the existing state of the art coupled C-N models may simulate N₂O emissions (e.g., Zaehle et al., 2011) but interactive NO_x (NO+NO₂=NO_x) emissions are not yet available. NO_x emissions are relevant for tropospheric ozone and aerosol chemistry (not N₂O, which does not react in the troposphere). The NASA ModelE2-YIBs framework already includes climate-dependent soil NO_x emissions (described in Section 3.7). We have already emphasized that NASA ModelE2-YIBs simulates the speciated interactive deposition of inorganic and organic nitrogen to the terrestrial biosphere in Section 3.7.

We strengthen the case for not yet incorporating coupled C-N into YIBs in Section 3.7 (Lines 540-543) through additional updated key references:

“However, the YIBs biosphere currently applies fixed nitrogen levels and does not yet account for the dynamic interactions between the carbon and nitrogen cycles, and the consequences for carbon assimilation, which are highly uncertain (e.g., Thornton et al., 2007; Koven et al., 2013; Thomas et al., 2013; Zaehle et al., 2014; Houlton et al., 2015).”

And in the Conclusions section (Lines 774-777):

“The model does not yet include a dynamic treatment of nitrogen and phosphorous availability because current schemes suffer from large uncertainties (Thornton et al., 2007; Zaehle et al., 2014; Houlton et al., 2015)”

Since the paper is already rather long, an additional paragraph detailing the state of C-N models, what we know and don't know, is not justified here.

As a last point, recent ‘state of the science’ carbon-chemistry-climate research on ozone vegetation damage effects on the carbon and water cycles used CLM and did not use CLM-CN (Lombardozzi et al., 2015).

Minor comments:

The physiology references are incorrect, the Collatz et al (1991) equations for photosynthesis are presented (equations 2-4), but Farquhar et al (1980) are cited. Why cite Collatz for the Ball-Berry model of stomatal conductance? Cite Ball et al (1987). And why use this model, later versions are available, e.g Medlyn et al 2011.

→ We have corrected the reference typos in the revised manuscript.

Testing alternative stomatal conductance models is way beyond the scope of this particular paper but will be a subject of future YIBs research, not least because it is critical for chemistry-climate interactions. We have added the following statement (Lines 219-221):

“In future work, we will investigate the carbon-chemistry-climate impacts of updated stomatal conductance models in YIBs (Berry et al., 2010; Pieruschka et al., 2010; Medlyn et al., 2011).”

The general definition of PFT is 'plant functional type', this should be unified through the manuscript as 'plant functional type', 'plant function type', and 'land cover type' are used interchangeably.

→ Corrected. We use “plant functional type” and the abbreviation PFT throughout the manuscript.

Figure 4 are not histograms, they are bar charts. To be histograms each x-axis should be on a single scale. For example plot 4c, intervals (from left to right) of 42, 17, 33, 50, 50, and 396 are all given the same distance on the x-axis. Also, there should be less or no space between the bars, the x-axis is a continuous variable. I suggest using box and whisker plots to represent these distributions.

→ We appreciate the referee's suggestion of the box and whisker plots, but those would be incapable of distinguishing PFTs as the colored bars. We now refer to Figure 4 as “bar charts”.

Reference

- Batjes, N. H.: Harmonized soil profile data for applications at global and continental scales: updates to the WISE database, *Soil Use Manage*, 25, 124-127, doi:10.1111/J.1475-2743.2009.00202.X, 2009.
- Berry, J. A., Beerling, D. J., and Franks, P. J.: Stomata: key players in the earth system, past and present, *Curr Opin Plant Biol*, 13, 233-240, doi:10.1016/J.Pbi.2010.04.013, 2010.
- Clark, D. B., Mercado, L. M., Sitch, S., Jones, C. D., Gedney, N., Best, M. J., Pryor, M., Rooney, G. G., Essery, R. L. H., Blyth, E., Boucher, O., Harding, R. J., Huntingford, C., and Cox, P. M.: The Joint UK Land Environment Simulator (JULES), model description - Part 2: Carbon fluxes and vegetation dynamics, *Geosci Model Dev*, 4, 701-722, doi:10.5194/Gmd-4-701-2011, 2011.
- Cox, P. M.: Description of the "TRIFFID" Dynamic Global Vegetation Model, Hadley Centre technical note 24, 2001.
- Friedlingstein, P., Andrew, R. M., Rogelj, J., Peters, G. P., Canadell, J. G., Knutti, R., Luderer, G., Raupach, M. R., Schaeffer, M., van Vuuren, D. P., and Le Quere, C.: Persistent growth of CO₂ emissions and implications for reaching climate targets, *Nat Geosci*, 7, 709-715, doi:10.1038/Ngeo2248, 2014.
- Friedlingstein, P., Cox, P., Betts, R., Bopp, L., Von Bloh, W., Brovkin, V., Cadule, P., Doney, S., Eby, M., Fung, I., Bala, G., John, J., Jones, C., Joos, F., Kato, T., Kawamiya, M., Knorr, W., Lindsay, K., Matthews, H. D., Raddatz, T., Rayner, P., Reick, C., Roeckner, E., Schnitzler, K. G., Schnur, R., Strassmann, K., Weaver, A. J., Yoshikawa, C., and Zeng, N.: Climate-carbon cycle feedback analysis: Results from the (CMIP)-M-4 model intercomparison, *J Climate*, 19, 3337-3353, doi:10.1175/Jcli3800.1, 2006.
- Houlton, B. Z., Marklein, A. R., and Bai, E.: Representation of nitrogen in climate change forecasts, *Nat Clim Change*, 5, 398-401, 2015.
- Huntzinger, D. N., Schwalm, C., Michalak, A. M., Schaefer, K., King, A. W., Wei, Y., Jacobson, A., Liu, S., Cook, R. B., Post, W. M., Berthier, G., Hayes, D., Huang, M., Ito, A., Lei, H., Lu, C., Mao, J., Peng, C. H., Peng, S., Poulter, B., Riccuito, D., Shi, X., Tian, H., Wang, W., Zeng, N., Zhao, F., and Zhu, Q.: The North American Carbon Program Multi-Scale Synthesis and Terrestrial Model Intercomparison Project - Part 1: Overview and experimental design, *Geosci Model Dev*, 6, 2121-2133, doi:10.5194/Gmd-6-2121-2013, 2013.
- Kattge, J. and co-authors: TRY - a global database of plant traits, *Global Change Biol*, 17, 2905-2935, doi:10.1111/J.1365-2486.2011.02451.X, 2011.
- Koven, C. D., Riley, W. J., Subin, Z. M., Tang, J. Y., Torn, M. S., Collins, W. D., Bonan, G. B., Lawrence, D. M., and Swenson, S. C.: The effect of vertically resolved soil biogeochemistry and alternate soil C and N models on C dynamics of CLM4, *Biogeosciences*, 10, 7109-7131, doi:10.5194/Bg-10-7109-2013, 2013.
- Lamarque, J. F., Shindell, D. T., Josse, B., Young, P. J., Cionni, I., Eyring, V., Bergmann, D., Cameron-Smith, P., Collins, W. J., Doherty, R., Dalsoren, S., Faluvegi, G., Folberth, G., Ghan, S. J., Horowitz, L. W., Lee, Y. H., MacKenzie, I. A., Nagashima, T., Naik, V., Plummer, D., Righi, M., Rumbold, S. T., Schulz, M., Skeie, R. B., Stevenson, D. S., Strode, S., Sudo, K., Szopa, S., Voulgarakis, A., and

- Zeng, G.: The Atmospheric Chemistry and Climate Model Intercomparison Project (ACCMIP): overview and description of models, simulations and climate diagnostics, *Geosci Model Dev*, 6, 179-206, doi:10.5194/Gmd-6-179-2013, 2013.
- Lombardozzi, D., Levis, S., Bonan, G., Hess, P. G., and Sparks, J. P.: The Influence of Chronic Ozone Exposure on Global Carbon and Water Cycles, *J Climate*, 28, 292-305, doi:10.1175/Jcli-D-14-00223.1, 2015.
- Luyssaert, S. and co-authors: CO₂ balance of boreal, temperate, and tropical forests derived from a global database, *Global Change Biol*, 13, 2509-2537, doi:10.1111/J.1365-2486.2007.01439.X, 2007.
- Medlyn, B. E., Duursma, R. A., Eamus, D., Ellsworth, D. S., Prentice, I. C., Barton, C. V. M., Crous, K. Y., de Angelis, P., Freeman, M., and Wingate, L.: Reconciling the optimal and empirical approaches to modelling stomatal conductance, *Global Change Biol*, 17, 2134-2144, doi:10.1111/J.1365-2486.2010.02375.X, 2011.
- Mercado, L. M., Bellouin, N., Sitch, S., Boucher, O., Huntingford, C., Wild, M., and Cox, P. M.: Impact of changes in diffuse radiation on the global land carbon sink, *Nature*, 458, 1014-1017, doi:10.1038/Nature07949, 2009.
- Mercado, L. M., Patino, S., Domingues, T. F., Fyllas, N. M., Weedon, G. P., Sitch, S., Quesada, C. A., Phillips, O. L., Aragao, L. E. O. C., Malhi, Y., Dolman, A. J., Restrepo-Coupe, N., Saleska, S. R., Baker, T. R., Almeida, S., Higuchi, N., and Lloyd, J.: Variations in Amazon forest productivity correlated with foliar nutrients and modelled rates of photosynthetic carbon supply, *Philos T R Soc B*, 366, 3316-3329, doi:10.1098/Rstb.2011.0045, 2011.
- Olson, D. M., Dinerstein, E., Wikramanayake, E. D., Burgess, N. D., Powell, G. V. N., Underwood, E. C., D'amico, J. A., Itoua, I., Strand, H. E., Morrison, J. C., Loucks, C. J., Allnutt, T. F., Ricketts, T. H., Kura, Y., Lamoreux, J. F., Wettengel, W. W., Hedao, P., and Kassem, K. R.: Terrestrial Ecoregions of the World: A New Map of Life on Earth, *Bioscience*, 51, 933-938, doi:10.1641/0006-3568(2001)051[0933:TEOTWA]2.0.CO;2, 2001.
- Piao, S. L., Sitch, S., Ciais, P., Friedlingstein, P., Peylin, P., Wang, X. H., Ahlstrom, A., Anav, A., Canadell, J. G., Cong, N., Huntingford, C., Jung, M., Levis, S., Levy, P. E., Li, J. S., Lin, X., Lomas, M. R., Lu, M., Luo, Y. Q., Ma, Y. C., Myneni, R. B., Poulter, B., Sun, Z. Z., Wang, T., Viovy, N., Zaehle, S., and Zeng, N.: Evaluation of terrestrial carbon cycle models for their response to climate variability and to CO₂ trends, *Global Change Biol*, 19, 2117-2132, doi:10.1111/Gcb.12187, 2013.
- Pieruschka, R., Huber, G., and Berry, J. A.: Control of transpiration by radiation, *P Natl Acad Sci USA*, 107, 13372-13377, doi:10.1073/Pnas.0913177107, 2010.
- Potter, C. S., Randerson, J. T., Field, C. B., Matson, P. A., Vitousek, P. M., Mooney, H. A., and Klooster, S. A.: Terrestrial Ecosystem Production - a Process Model-Based on Global Satellite and Surface Data, *Global Biogeochem Cy*, 7, 811-841, doi:10.1029/93gb02725, 1993.
- Schaefer, K., Collatz, G. J., Tans, P., Denning, A. S., Baker, I., Berry, J., Prihodko, L., Suits, N., and Philpott, A.: Combined Simple Biosphere/Carnegie-Ames-Stanford Approach terrestrial carbon cycle model, *J. Geophys. Res.*, 113, G03034, doi:10.1029/2007jg000603, 2008.

- Schaefer, K. and co-authors: A model-data comparison of gross primary productivity: Results from the North American Carbon Program site synthesis, *J. Geophys. Res.*, 117, G03010, doi:10.1029/2012jg001960, 2012.
- Shindell, D. T., Lamarque, J. F., Schulz, M., Flanner, M., Jiao, C., Chin, M., Young, P. J., Lee, Y. H., Rotstayn, L., Mahowald, N., Milly, G., Faluvegi, G., Balkanski, Y., Collins, W. J., Conley, A. J., Dalsoren, S., Easter, R., Ghan, S., Horowitz, L., Liu, X., Myhre, G., Nagashima, T., Naik, V., Rumbold, S. T., Skeie, R., Sudo, K., Szopa, S., Takemura, T., Voulgarakis, A., Yoon, J. H., and Lo, F.: Radiative forcing in the ACCMIP historical and future climate simulations, *Atmos Chem Phys*, 13, 2939-2974, doi:10.5194/Acp-13-2939-2013, 2013a.
- Shindell, D. T., Pechony, O., Voulgarakis, A., Faluvegi, G., Nazarenko, L., Lamarque, J. F., Bowman, K., Milly, G., Kovari, B., Ruedy, R., and Schmidt, G. A.: Interactive ozone and methane chemistry in GISS-E2 historical and future climate simulations, *Atmos Chem Phys*, 13, 2653-2689, doi:10.5194/Acp-13-2653-2013, 2013b.
- Sitch, S., Cox, P. M., Collins, W. J., and Huntingford, C.: Indirect radiative forcing of climate change through ozone effects on the land-carbon sink, *Nature*, 448, 791-794, doi:10.1038/Nature06059, 2007.
- Sitch, S., Friedlingstein, P., Gruber, N., Jones, S. D., Murray-Tortarolo, G., Ahlström, A., Doney, S. C., Graven, H., Heinze, C., Huntingford, C., Levis, S., Levy, P. E., Lomas, M., Poulter, B., Viovy, N., Zaehle, S., Zeng, N., Arneth, A., Bonan, G., Bopp, L., Canadell, J. G., Chevallier, F., Ciais, P., Ellis, R., Gloor, M., Peylin, P., Piao, S. L., Quéré, C. L., Smith, B., Zhu, Z., and Myneni, R.: Recent trends and drivers of regional sources and sinks of carbon dioxide, *Biogeosciences*, 12, 653-679, 2015.
- Thomas, R. Q., Zaehle, S., Templer, P. H., and Goodale, C. L.: Global patterns of nitrogen limitation: confronting two global biogeochemical models with observations, *Global Change Biol*, 19, 2986-2998, doi:10.1111/Gcb.12281, 2013.
- Thornton, P. E., Lamarque, J. F., Rosenbloom, N. A., and Mahowald, N. M.: Influence of carbon-nitrogen cycle coupling on land model response to CO₂ fertilization and climate variability, *Global Biogeochem Cy*, 21, Gb4018, doi:10.1029/2006gb002868, 2007.
- Unger, N.: Human land-use-driven reduction of forest volatiles cools global climate, *Nat Clim Change*, 4, 907-910, doi:10.1038/Nclimate2347, 2014a.
- Unger, N.: Isoprene emission variability through the twentieth century, *J. Geophys. Res.*, 118, 13606-13613, doi:10.1002/2013jd020978, 2013.
- Unger, N.: On the role of plant volatiles in anthropogenic global climate change, *Geophys Res Lett*, 41, 8563-8569, doi:10.1002/2014gl061616, 2014b.
- Unger, N., Harper, K., Zheng, Y., Kiang, N. Y., Aleinov, I., Arneth, A., Schurgers, G., Amelynck, C., Goldstein, A., Guenther, A., Heinesch, B., Hewitt, C. N., Karl, T., Laffineur, Q., Langford, B., McKinney, K. A., Misztal, P., Potosnak, M., Rinne, J., Pressley, S., Schoon, N., and Serça, D.: Photosynthesis-dependent isoprene emission from leaf to planet in a global carbon-chemistry-climate model, *Atmos. Chem. Phys.*, 13, 10243-10269, doi:10.5194/acp-13-10243-2013, 2013a.
- Unger, N., Harper, K., Zheng, Y., Kiang, N. Y., Aleinov, I., Arneth, A., Schurgers, G., Amelynck, C., Goldstein, A., Guenther, A., Heinesch, B., Hewitt, C. N., Karl, T., Laffineur, Q., Langford, B., McKinney, K. A., Misztal, P., Potosnak, M., Rinne, J., Pressley, S., Schoon, N., and Serça, D.: Photosynthesis-dependent isoprene emission

- from leaf to planet in a global carbon–chemistry–climate model, *Atmos. Chem. Phys.*, 13, 17717-17791, doi:10.5194/acp-13-10243-2013, 2013b.
- Unger, N. and Yue, X.: Strong chemistry- climate feedbacks in the Pliocene, *Geophys. Res. Lett.*, 41, 527-533, doi:10.1002/2013gl058773, 2014.
- Wutzler, T. and Reichstein, M.: Soils apart from equilibrium - consequences for soil carbon balance modelling, *Biogeosciences*, 4, 125-136, 2007.
- Yue, X. and Unger, N.: Ozone vegetation damage effects on gross primary productivity in the United States, *Atmos. Chem. Phys.*, 14, 9137-9153, doi:10.5194/acp-14-9137-2014, 2014.
- Yue, X., Unger, N., Keenan, T. F., Zhang, X., and Vogel, C. S.: Probing the past 30-year phenology trend of U.S. deciduous forests, *Biogeosciences Discuss.*, 12, 6037-6080, doi:10.5194/bgd-12-6037-2015, 2015.
- Zaehle, S., Ciais, P., Friend, A. D., and Prieur, V.: Carbon benefits of anthropogenic reactive nitrogen offset by nitrous oxide emissions, *Nat Geosci*, 4, 601-605, doi:10.1038/Ngeo1207, 2011.
- Zaehle, S., Medlyn, B. E., De Kauwe, M. G., Walker, A. P., Dietze, M. C., Hickler, T., Luo, Y. Q., Wang, Y. P., El-Masri, B., Thornton, P., Jain, A., Wang, S. S., Warland, D., Weng, E. S., Parton, W., Iversen, C. M., Gallet-Budynek, A., McCarthy, H., Finzi, A. C., Hanson, P. J., Prentice, I. C., Oren, R., and Norby, R. J.: Evaluation of 11 terrestrial carbon-nitrogen cycle models against observations from two temperate Free-Air CO₂ Enrichment studies, *New Phytol*, 202, 803-822, doi:10.1111/Nph.12697, 2014.
- Zheng, Y., Unger, N., Barley, M., and Yue, X.: Relationships between photosynthesis and formaldehyde as a probe of isoprene emission, *Atmos. Chem. Phys. Discuss.*, 15, 11763-11797, 2015.

**The Yale Interactive terrestrial Biosphere Model version 1.0: description,
evaluation and implementation into NASA GISS ModelE2**

X. Yue and N. Unger

School of Forestry and Environment Studies, Yale University, New Haven, Connecticut
06511, USA

Abstract

The land biosphere, atmospheric chemistry and climate are intricately interconnected, yet the modeling of carbon-climate and chemistry-climate interactions have evolved as entirely separate research communities. We describe the Yale Interactive terrestrial Biosphere (YIBs) model version 1.0, a land carbon cycle model that has been developed for coupling to the NASA Goddard Institute for Space Studies (GISS) ModelE2 global chemistry-climate model. The YIBs model adapts routines from the mature TRIFFID and CASA models to simulate interactive carbon assimilation, allocation, and autotrophic and heterotrophic respiration. Dynamic daily leaf area index is simulated based on carbon allocation and temperature- and drought-dependent prognostic phenology. YIBs incorporates a semi-mechanistic ozone vegetation damage scheme. Here, we validate the present day YIBs land carbon fluxes for three increasingly complex configurations: (i) off-line local site-level (ii) off-line global forced with WFDEI (WATCH Forcing Data methodology applied to ERA-Interim data) meteorology (iii) on-line coupled to the NASA ModelE2 (NASA ModelE2-YIBs). Off-line YIBs has hourly and on-line YIBs has half-hourly temporal resolution. The large observational database used for validation includes carbon fluxes from 145 flux tower sites and multiple satellite products. At the site level, YIBs simulates reasonable seasonality (correlation coefficient $R > 0.8$) of gross primary productivity (GPP) at 121 out of 145 sites with biases in magnitude ranging from -19% to 7% depending on plant functional type. On the global scale, the off-line model simulates an annual GPP of 125 ± 3 petagrams of carbon (Pg C) and net ecosystem exchange (NEE) of -2.5 ± 0.7 Pg C for 1982-2011, with seasonality and spatial distribution consistent with the satellite observations. We assess present day global ozone vegetation damage using the off-line YIBs configuration. Ozone damage reduces global GPP by 2-5% annually with regional extremes of 4-10% in East Asia. The on-line model simulates annual GPP of 123 ± 1 Pg C and NEE of -2.7 ± 0.7 Pg C. NASA ModelE2-YIBs is a useful new tool to investigate coupled interactions between the land carbon cycle, atmospheric chemistry, and climate change.

Keywords: terrestrial biosphere model, carbon cycle, photosynthesis, ozone, phenology, gross primary productivity, net ecosystem exchange.

Xu Yue 6/24/15 3:34 PM

Deleted: inextricably

Xu Yue 6/24/15 3:34 PM

Deleted: .

Xu Yue 6/24/15 3:34 PM

Deleted: function

Xu Yue 6/24/15 3:34 PM

Deleted: .

1. Introduction

The terrestrial biosphere interacts with the atmosphere through the exchanges of energy, carbon, reactive gases, water, and momentum fluxes. Forest ecosystems absorb an estimated 120 petagrams of carbon (Pg C) per year from the atmosphere (Beer et al., 2010) and mitigate about one quarter of the anthropogenic carbon dioxide (CO₂) emissions (Friedlingstein et al., 2014). This carbon assimilation is sensitive to human-caused perturbations including climate change and land use change (Zhao and Running, 2010; Houghton et al., 2012), and is affected by atmospheric pollutants such as ozone and aerosols (Sitch et al., 2007; Mercado et al., 2009). Over the past 2-3 decades, a number of terrestrial biosphere models have been developed as tools to quantify the present-day global carbon budget in conjunction with available but sparse observations (e.g., Jung et al., 2009), to understand the relationships between terrestrial biospheric fluxes and environmental conditions (e.g., Zeng et al., 2005), to attribute drivers of trends in the carbon cycle during the anthropogenic era (e.g., Sitch et al., 2015), and to project future changes in the land biosphere and the consequences for regional and global climate change (e.g., Friedlingstein et al., 2006).

Emerging research identifies climatically-relevant interactions between the land biosphere and atmospheric chemistry (e.g., Huntingford et al., 2011). For instance, stomatal uptake is an important sink of tropospheric ozone (Val Martin et al., 2014), but damages photosynthesis, reduces plant growth and biomass accumulation, limits crop yields, and affects stomatal control over plant transpiration of water vapor between the leaf surface and atmosphere (Ainsworth et al., 2012; Hollaway et al., 2012). The indirect CO₂ radiative forcing due to the vegetation damage effects of anthropogenic ozone increases since the industrial revolution may be as large as +0.4 W m⁻² (Sitch et al., 2007), which is 25% of the magnitude of the direct CO₂ radiative forcing over the same period, and of similar magnitude to the direct ozone radiative forcing. Atmospheric oxidation of biogenic volatile organic compound (BVOC) emissions affects surface air quality and exerts additional regional and global chemical climate forcings (Scott et al., 2014; Unger, 2014a, b). Fine mode atmospheric pollution particles affect the land biosphere by changing the physical climate state and through diffuse radiation

fertilization (Mercado et al., 2009; Mahowald, 2011). Land plant phenology has experienced substantial changes in the last few decades (Keenan et al., 2014), possibly influencing both ozone deposition and BVOC emissions through the extension of growing seasons. These coupled interactions are often not adequately represented in current generation land biosphere models or global chemistry-climate models. Global land carbon cycle models often prescribe off-line ozone and aerosol fields (e.g., Sitch et al., 2007; Mercado et al., 2009), and global chemistry-climate models often prescribe fixed off-line vegetation fields (e.g., Lamarque et al., 2013; Shindell et al., 2013a). However, multiple mutual feedbacks occur between vegetation physiology and reactive atmospheric chemical composition that are completely neglected using these previous off-line approaches. Model frameworks are needed that fully 2-way couple the land carbon cycle and atmospheric chemistry, and simulate the consequences for climate change.

Our objective is to present the description and present-day evaluation of the Yale Interactive terrestrial Biosphere (YIBs) model version 1.0 that has been developed for the investigation of carbon-chemistry-climate interactions. The YIBs model can be used in three configurations: (i) off-line local site-level (ii) off-line global forced with WFDEI (WATCH Forcing Data methodology applied to ERA-Interim data) meteorology (iii) on-line coupled to the latest frozen version of the NASA GISS ModelE2 (Schmidt et al., 2014). The global climate model represents atmospheric gas-phase and aerosol chemistry, cloud, radiation, and land surface processes, and has been widely used for studies of atmospheric components, climate change, and their interactions (Schmidt et al., 2006; Koch et al., 2011; Unger, 2011; Shindell et al., 2013b; Miller et al., 2014). To our knowledge, this study represents the first description and validation of an interactive climate-sensitive closed land carbon cycle in NASA ModelE2. The impacts of the updated vegetation scheme on the chemistry and climate simulations in NASA ModelE2 will be addressed in other on-going research. Section 2 describes the observational datasets used to evaluate YIBs land carbon cycle performance. Section 3 describes physical parameterizations of the vegetation model. Section 4 explains the model set up

Xu Yue 6/24/15 3:34 PM

Deleted: In this study, we

Xu Yue 6/24/15 3:34 PM

Deleted: Model (YIBs)

Xu Yue 6/24/15 3:34 PM

Deleted: The goal of

Xu Yue 6/24/15 3:34 PM

Deleted: is to evaluate

Xu Yue 6/24/15 3:34 PM

Deleted: YIBs

Xu Yue 6/24/15 3:34 PM

Deleted: fluxes and vegetation behavior for the present day

and simulations in three configurations. Section 5 presents the results of the model evaluation and section 6 summarizes the model performance.

1.1 YIBs design strategy

Many land carbon cycle models already exist (e.g. Sitch et al., 2015 and references therein; Schaefer et al., 2012 and references therein). We elected to build YIBs in a step-by-step process such that our research group has intimate familiarity with the underlying scientific processes, rather than adopting an existing model as a “black box”. This unconventional interdisciplinary approach is important for discerning the complex mutual feedbacks between atmospheric chemistry and the land carbon sink under global change. The development of YIBs land carbon cycle model has proceeded in three main steps. The first step was the implementation of vegetation biophysics, photosynthesis-dependent BVOC emissions and ozone vegetation damage that have been extensively documented, validated and applied in 7 previous publications (Unger, 2013; Unger et al., 2013; Unger, 2014a, b; Unger and Yue, 2014; Yue and Unger, 2014; Zheng et al., 2015). The second step was the selection of the YIBs default phenology scheme based on rigorous inter-comparison of 13 published phenological models (Yue et al., 2015a). This study represents the third step to simulate the closed climate-sensitive land carbon cycle: implementation of interactive carbon assimilation, allocation, autotrophic and heterotrophic respiration, and dynamic tree growth (changes in both height and LAI). For this third step, we purposefully select the mature, well-supported, well-established, readily available and accessible community algorithms: TRIFFID (Cox, 2001; Clark et al., 2011) and the Carnegie-Ames-Stanford Approach (CASA) (Potter et al., 1993; Schaefer et al., 2008). TRIFFID has demonstrated previous usage in carbon-chemistry-climate interactions research.

2. Observational datasets for validation

2.1 Site-level measurements

To validate the YIBs model, we use eddy covariance measurements from 145 flux tower sites (Fig. 1), which are collected by the North American Carbon Program (Schaefer et al., 2012), (K. Schaefer, personal communication) and downloaded from the FLUXNET (<http://fluxnet.ornl.gov>) network. Among these sites, 138 are located in the Northern Hemisphere, with 74 in Europe, 38 in U.S., and 24 in Canada (Table S1). Sites on other continents are limited. Most of the sites have one dominant plant functional type (PFT), including 54 sites of evergreen needleleaf forests (ENF), 20 deciduous broadleaf forests (DBF), 9 evergreen broadleaf forests (EBF), 28 grasslands, 18 shrublands, and 16 croplands. We attribute sites with mixed forest to the ENF as these sites are usually at high latitudes. Each site dataset provides hourly or half-hourly measurements of carbon fluxes, including gross primary productivity (GPP) and net ecosystem exchange (NEE), and CO₂ concentrations and meteorological variables, such as surface air temperature, relative humidity, wind speed, and shortwave radiation.

2.2 Global measurements

We use global tree height, leaf area index (LAI), GPP, net primary productivity (NPP), and phenology datasets to validate the vegetation model. Canopy height is retrieved using 2005 remote sensing data from the Geoscience Laser Altimeter System (GLAS) aboard ICESat satellite (Simard et al., 2011). LAI measurements for 1982-2011 are derived using the Normalized Difference Vegetation Index (NDVI) from Global Inventory Modeling and Mapping Studies (GIMMS) (Zhu et al., 2013). Global GPP observations of 1982-2011 are estimated based on the upscaling of FLUXNET eddy covariance data with a biosphere model (Jung et al., 2009). This product was made to reproduce a model (LPJmL) using the fraction of absorbed PAR simulated in LPJmL. As a comparison, we also use GPP observations of 1982-2008 derived based on FLUXNET, satellite, and meteorological observations (Jung et al., 2011), which is about 10% lower than that of Jung et al. (2009). The NPP for 2000-2011 is derived using remote sensing data from Moderate Resolution Imaging Spectroradiometer (MODIS) (Zhao et al., 2005). We use the global retrieval of greenness onset derived from the Advanced Very High Resolution

Xu Yue 6/24/15 3:34 PM

Deleted: and

Xu Yue 6/24/15 3:34 PM

Deleted: function

Xu Yue 6/24/15 3:34 PM

Deleted: . Global GPP observations of 1982-2011 are estimated based on the upscaling of FLUXNET eddy covariance data with a biosphere model (Jung et al., 2009). As a comparison, we also use GPP observations of 1982-2008 derived based on FLUXNET, satellite, and meteorological observations

Radiometer (AVHRR) and the MODIS data from 1982 to 2011 (Zhang et al., 2014). All datasets are interpolated to the $1^\circ \times 1^\circ$ off-line model resolution for comparisons.

3. YIBs model description

3.1 Vegetation biophysics

YIBs calculates carbon uptake for 9 PFTs: tundra, C3/C4 grass, shrubland, DBF, ENF, EBF, and C3/C4 cropland (Table 1). In the gridded large-scale model applications, each model PFT fraction in the vegetated part of each grid cell represents a single canopy. The vegetation biophysics simulates C3 and C4 photosynthesis with the well-established Michealis-Menten enzyme-kinetics scheme (Farquhar et al., 1980; von Caemmerer and Farquhar, 1981) and the stomatal conductance model of Ball and Berry (Ball et al., 1987). The total leaf photosynthesis (A_{tot} , $\mu\text{mol m}^{-2} [\text{leaf}] \text{ s}^{-1}$) is limited by one of three processes: (i) the capacity of the ribulose 1,5-bisphosphate (RuBP) carboxylase-oxygenase enzyme (Rubisco) to catalyze carbon fixation (J_c); (ii) the capacity of the Calvin cycle and the thylakoid reactions to regenerate RuBP supported by electron transport (J_e); (iii) the capacity of starch and sucrose synthesis to regenerate inorganic phosphate for photo-phosphorylation in C3 plants and phosphoenolpyruvate (PEP) in C4 plants (J_s).

$$A_{tot} = \min(J_c, J_e, J_s) \quad (1)$$

The J_c , J_e , and J_s are parameterized as functions of environmental variables (e.g. temperature, radiation, and CO_2 concentrations) and the maximum carboxylation capacity (V_{cmax} , $\mu\text{mol m}^{-2} \text{ s}^{-1}$) (Collatz et al., 1991; Collatz et al., 1992):

$$J_c = \begin{cases} V_{cmax} \left(\frac{c_i - \Gamma_*}{c_i + K_c(1 + O_i / K_o)} \right) & \text{for C3 plant} \\ V_{cmax} & \text{for C4 plant} \end{cases} \quad (2)$$

Unknown

Field Code Changed

Xu Yue 6/24/15 3:34 PM

Deleted: Previously, we presented and evaluated an off-line regional version of YIBs that was applied to assess ozone damage effects on GPP in the U.S. (Yue and Unger, 2014); and an on-line global version of YIBs that was used to investigate BVOC-chemistry-climate interactions (Unger, 2013; Unger and Yue, 2014). Here, we describe the recent updated functionalities of the YIBs model that now represents the complete land carbon cycle: interactive carbon assimilation, allocation, autotrophic and heterotrophic respiration, and dynamic tree growth (changes in both height and LAI).

Xu Yue 6/24/15 3:34 PM

Deleted: plant functional types (

Xu Yue 6/24/15 3:34 PM

Deleted:):

Xu Yue 6/24/15 3:34 PM

Deleted: (Collatz et al., 1991).

Xu Yue 6/24/15 3:34 PM

Deleted: (Farquhar et al., 1980):

$$J_e = \begin{cases} a_{leaf} \cdot PAR \cdot \alpha \cdot \left(\frac{c_i - \Gamma_*}{c_i + 2\Gamma_*} \right) & \text{for C3 plant} \\ a_{leaf} \cdot PAR \cdot \alpha & \text{for C4 plant} \end{cases} \quad (3)$$

$$J_s = \begin{cases} 0.5V_{cmax} & \text{for C3 plant} \\ K_s \cdot V_{cmax} \cdot \frac{c_i}{P_s} & \text{for C4 plant} \end{cases} \quad (4)$$

where c_i and O_i are the leaf internal partial pressure (Pa) of CO_2 and oxygen, Γ_* (Pa) is the CO_2 compensation point, K_c and K_o (Pa) are Michaelis-Menten parameters for the carboxylation and oxygenation of rubisco. The parameters K_c , K_o , and Γ_* vary with temperature according to a Q_{10} function. PAR ($\mu\text{mol m}^{-2} \text{s}^{-1}$) is the incident photosynthetically active radiation, a_{leaf} is leaf-specific light absorbance, and α is intrinsic quantum efficiency. P_s is the ambient pressure and K_s is a constant set to 4000 following Oleson et al. (2010). V_{cmax} is a function of the optimal V_{cmax} at 25 °C (V_{cmax25}) based on a Q_{10} function.

Net carbon assimilation (A_{net}) of leaf is given by:

$$A_{net} = A_{tot} - R_d \quad (5)$$

where R_d is the rate of dark respiration set to 0.011 V_{cmax} for C3 plants (Farquhar et al., 1980) and 0.025 V_{cmax} for C4 plants (Clark et al., 2011). The stomatal conductance of water vapor (g_s in $\text{mol [H}_2\text{O]} \text{ m}^{-2} \text{s}^{-1}$) is dependent on net photosynthesis:

$$g_s = m \frac{A_{net} \cdot RH}{c_s} + b \quad (6)$$

where m and b are the slope and intercept derived from empirical fitting to the Ball and Berry stomatal conductance equations, RH is relative humidity, and c_s is the CO_2 concentration at the leaf surface. In the model, the slope m is influenced by water stress,

so that drought decreases photosynthesis by affecting stomatal conductance. Appropriate photosynthesis parameters for different PFTs are taken from Friend and Kiang (2005) and the Community Land Model (Oleson et al., 2010) with updates from Bonan et al. (2011) (Table 1). In future work, we will investigate the carbon-chemistry-climate impacts of updated stomatal conductance models in YIBs (Berry et al., 2010; Pieruschka et al., 2010; Medlyn et al., 2011).

The coupled equation system of photosynthesis, stomatal conductance and CO₂ diffusive flux transport equations form a cubic in A_{net} that is solved analytically (Baldocchi, 1994). A simplified but realistic representation of soil water stress β is included in the vegetation biophysics following the approach of Porporato et al. (2001). The algorithm reflects the relationship between soil water amount and the extent of stomatal closure ranging from no water stress to the soil moisture stress onset point (s^*) through to the wilting point (s_{wilt}). Stomatal conductance is reduced linearly between the PFT-specific values of s^* and s_{wilt} based on the climate model's soil water volumetric saturation in 6 soil layers (Unger et al., 2013).

The canopy radiative transfer scheme divides the canopy into an adaptive number of layers (typically 2-16) for light stratification. Each canopy layer distinguishes sunlit and shaded portions of leaves, so that the direct and diffuse photosynthetically active radiation (PAR) is used for carbon assimilation respectively (Spitters et al., 1986). The leaf photosynthesis is then integrated over all canopy layers to generate the GPP:

$$GPP = \int_0^{LAI} A_{tot} dL \quad (7)$$

3.2 Leaf phenology

Phenology determines the annual cycle of LAI. Plant phenology is generally controlled by temperature, water availability, and photoperiod (Richardson et al., 2013). For deciduous trees, the timing of budburst is sensitive to temperature (Vitasse et al., 2009) and the autumn senescence is related to both temperature and photoperiod (Delpierre et al., 2009). For small trees and grasses, such as tundra, savanna, and shrubland, phenology

Xu Yue 6/24/15 3:34 PM

Deleted: c_i

is controlled by temperature and/or soil moisture, depending on the species type and locations of the vegetation (Delbart and Picard, 2007; Liu et al., 2013). In the YIBs model, leaf phenology is updated on a daily basis. For the YIBs model, we have extended the phenology scheme proposed by Kim and Wang (2005), based on long-term measurements of leaf phenology at 5 U.S. sites (Yue et al., 2015a, hereinafter Y2015) and GPP at the 145 flux tower sites. A summary of the phenological parameters adopted is listed in Table 2.

3.2.1 Deciduous broadleaf forest (DBF)

We predict spring phenology of DBF using the cumulative thermal summation (White et al., 1997). The accumulative growing degree day (GDD) is calculated for the n th day from winter solstice if the 10-day average air temperature T_{10} is higher than a base temperature T_b :

$$GDD = \sum_{i=1}^n \max(T_{10} - T_b, 0) \quad (8)$$

Here T_b is set to 5°C as that in Murray et al. (1989). The onset of greenness is triggered if the GDD exceeds a threshold value G_b and a temperature-dependent phenological factor f_T is calculated as follows:

$$f_T = \begin{cases} \min\left(1, \frac{GDD - G_b}{L_g}\right), & \text{if } GDD \geq G_b \\ 0, & \text{otherwise} \end{cases} \quad (9)$$

Following Murray et al. (1989), the threshold $G_b = a + b \exp(r \cdot NCD)$ is dependent on the number of chill days (NCD), which is calculated as the total days with < 5°C from winter solstice.

The autumn phenology is more uncertain than budburst because it is affected by both temperature and photoperiod (White et al., 1997; Delpierre et al., 2009). For the

temperature dependent phenology, we adopted the cumulative cold summation method (Dufrene et al., 2005; Richardson et al., 2006), which calculates the accumulative falling degree day (FDD) for the m th day from summer solstice as follows,

$$FDD = \sum_{i=1}^m \min(T_{10} - T_s, 0) \quad (10)$$

where T_s is 20°C as that in Dufrene et al. (2005). Similar to the budburst process, we determine autumn phenological factor based on a fixed threshold F_s :

$$f_T = \begin{cases} \max\left(0, 1 + \frac{FDD - F_s}{L_f}\right), & \text{if } FDD \leq F_s \\ 1, & \text{otherwise} \end{cases} \quad (11)$$

In addition, we assume photoperiod regulates leaf senescence as follows,

$$f_P = \begin{cases} \max\left(0, \frac{P - P_i}{P_x - P_i}\right), & \text{if } P \leq P_x \\ 1, & \text{otherwise} \end{cases} \quad (12)$$

where f_P is the photoperiod-limited phenology. P is daylength in minutes. P_i and P_x are the lower and upper limits of daylength for the period of leaf fall. Finally, the autumn phenology of DBF is determined as the product of f_T (Equation 11) and f_P (Equation 12). Both the spring and autumn phenology schemes have been evaluated with extensive ground records over the U.S. in Y2015.

3.2.2 Shrubland

Shrub phenology is sensitive to temperature and/or water availability. We calculate correlation coefficients between observed GPP and soil meteorology at 18 shrub sites (Fig. 2). For 10 sites with annual mean soil temperature < 9 °C, the GPP-temperature correlations are close to 1 while the GPP-moisture correlations are all negative (Fig. 2a),

suggesting that temperature is the dominant phenological driver for these plants. In contrast, for 8 sites with average soil temperature $> 14^{\circ}\text{C}$, GPP-moisture correlations are positive and usually higher than the GPP-temperature correlations, indicating that phenology is primarily regulated by water availability at climatologically warm areas. The wide temperature gap ($9\text{--}14^{\circ}\text{C}$) is due to the limit in the availability of shrub sites. Here, we select a tentative threshold of 12°C to distinguish cold and drought species. We also try to identify phenological drivers based on soil moisture thresholds but find that both temperature- and drought-dependent phenology may occur at moderately dry conditions (Fig. 2b).

In the model, we apply the temperature-dependent phenology f_T for shrubland, if the site has annual mean soil temperature $< 12^{\circ}\text{C}$. We use the same f_T as that for DBF (Equations 9 and 11), due to the lack of long-term phenology measurements at the shrub sites. However, if the soil temperature is $> 12^{\circ}\text{C}$, the plant growth is controlled by drought-limit phenology f_D instead:

$$f_D = \begin{cases} \max\left(0, \frac{\beta_{10} - \beta_{\min}}{\beta_{\max} - \beta_{\min}}\right), & \text{if } \beta_{10} \leq \beta_{\max} \\ 1, & \text{otherwise} \end{cases} \quad (13)$$

where β_{10} is 10-day average water stress calculated based on soil moisture, soil ice fraction, and root fraction of each soil layer (Porporato et al., 2001). The value of β_{10} changes from 0 to 1, with lower value indicating drier soil. Two thresholds, β_{\max} and β_{\min} , represent the upper and lower thresholds that trigger the drought limit for woody species. The values of these thresholds are set to $\beta_{\max} = 1$ and $\beta_{\min} = 0.4$ so that the predicted phenology has the maximum correlations with the observed GPP seasonality (Fig. S1a). The shrub phenology applies for shrubland in tropical and subtropical areas, as well as tundra at the subarctic regions, though the phenology of the latter is usually dependent on temperature alone because the climatological soil temperature is $< 12^{\circ}\text{C}$.

3.2.3 Grassland

In the model, we consider temperature-dependent phenology for grassland based on soil temperature (ST) accumulation (White et al., 1997):

$$SGDD = \sum_{i=1}^n \max(ST_{10} - ST_b, 0) \quad (14)$$

where ST_{10} is 10-day average soil temperature and $ST_b = 0$ °C. Similar to DBF, the onset of grass greenness is triggered if $SGDD$ is higher than a threshold value SG_b :

$$f_T = \begin{cases} \min\left(1, \frac{SGDD - SG_b}{SL_g}\right), & \text{if } SGDD \geq SG_b \\ 0, & \text{otherwise} \end{cases} \quad (15)$$

where SL_g determines the grow length of grass. Both SG_b and SL_g are calibrated based on observed GPP seasonality at FLUXNET sites (Table 2). Grass phenology at warm sites is also sensitive to water stress (Fig. 2c). We apply the same drought-limit phenology f_D as shrubland (Equation 13) for grassland but with calibrated threshold $\beta_{\max} = 0.9$ and $\beta_{\min} = 0.3$ (Fig. S1b). Different from shrubland whose phenology is dominated by drought when $ST > 12$ °C (Fig. 2a), grassland phenology is jointly affected by temperature and soil moisture (Fig. 2c). As a result, the final phenology for grassland at warm regions is the minimum of f_T and f_D .

3.2.4 Other PFTs

YIBs considers two evergreen PFTs, ENF at high latitudes and EBF in tropical areas. Observations do suggest that evergreen trees experience seasonal changes in LAI, following temperature variations and/or water availability (Doughty and Goulden, 2008; Schuster et al., 2014). However, due to the large uncertainty of evergreen phenology, we set a constant phenology factor of 1.0 for these species, following the approach adopted in other process-based vegetation models (Bonan et al., 2003; Sitch et al., 2003). We implement a parameterization for the impact of cold temperature (frost hardening) on the maximum carboxylation capacity (V_{cmax}) so as to reduce cold injury for ENF during

winter (Hanninen and Kramer, 2007). EBF may experience reduced photosynthesis during the dry season through the effects of water stress on stomatal conductance (Jones et al., 2014).

Crop phenology depends on planting and harvesting dates. In YIBs, we apply a global dataset of crop planting and harvesting dates (Sacks et al., 2010; Unger et al., 2013). Crop budburst occurs at the plant date and the crop continues to grow for a period of 30 days until reaching full maturity ($f = 1$). The crop leaves begin to fall 15 days prior to the harvest date, after which phenology is set to 0. A similar treatment has been adopted in CLM_v model (Bonan et al., 2003). Thus, crop productivity but not crop phenology is sensitive to the imposed meteorological forcings.

3.3 Carbon allocation

We adopt the autotrophic respiration and carbon allocation scheme applied in the dynamic global vegetation model (DGVM) TRIFFID (Cox, 2001; Clark et al., 2011). On a daily basis, the plant LAI is updated as follows:

$$LAI = f \cdot LAI_b \quad (16)$$

where f is the phenological factor, and LAI_b is the biomass-balanced (or available maximum) LAI related to tree height. LAI_b is dependent on the vegetation carbon content C_{veg} , which is the sum of carbon from leaf (C_l), root (C_r), and stem (C_w):

$$C_{veg} = C_l + C_r + C_w \quad (17)$$

where each carbon component is a function of LAI_b :

$$C_l = \sigma_l \cdot LAI \quad (18a)$$

$$C_r = \sigma_r \cdot LAI_b \quad (18b)$$

$$C_w = a_{wt} \cdot LAI_b^{b_{wt}} \quad (18c)$$

Xu Yue 6/24/15 3:34 PM

Deleted: Community Land Model (

Xu Yue 6/24/15 3:34 PM

Deleted:)

431

432 here σ_l is the specific leaf carbon density. a_{wl} and b_{wl} are PFT-specified allometric
 433 parameters (Table 1). The vegetation carbon content C_{veg} is updated every 10 days based
 434 on the carbon balance of assimilation, respiration, and litter fall.

435

$$436 \quad \frac{dC_{veg}}{dt} = (1 - \lambda) \cdot NPP - \Lambda_l \quad (19)$$

437

438 The net primary productivity (NPP) is the net carbon uptake:

439

$$440 \quad NPP = GPP - R_a \quad (20)$$

441

442 here GPP is the total photosynthesis rate integrated over LAI. Autotrophic respiration
 443 (R_a) is split into maintenance (R_{am}) and growth respiration (R_{ag}) (Clark et al., 2011):

444

$$445 \quad R_a = R_{am} + R_{ag} \quad (21)$$

446

447 The maintenance respiration is calculated based on nitrogen content in leaf (N_l), root (N_r),
 448 and stem (N_w) as follows,

449

$$450 \quad R_{am} = 0.012 R_d \left(\beta + \frac{N_r + N_w}{N_l} \right) \quad (22)$$

451

452 where R_d is the dark respiration of leaf, which is dependent on leaf temperature and is
 453 integrated over whole canopy LAI. The factor of 0.012 is the unit conversion from mol
 454 CO₂ m⁻² s⁻¹ to kg C m⁻² s⁻¹ and β is water stress representing soil water availability. The
 455 nitrogen contents are given by:

456

$$457 \quad N_l = n_0 \cdot C_l \quad (23a)$$

$$458 \quad N_r = n_{rl} \cdot n_0 \cdot C_r \quad (23b)$$

Xu Yue 6/24/15 3:34 PM

Deleted: $R_{am} = 0.012 R_{dc} \left(\beta + \frac{N_r + N_w}{N_l} \right)$

Unknown

Field Code Changed

Xu Yue 6/24/15 3:34 PM

Deleted: R_{dc}

$$N_w = n_{wl} \cdot n_0 \cdot \eta \cdot H \cdot LAI \quad (23c)$$

here n_0 is leaf nitrogen concentration, n_{rl} and n_{wl} are ratios of nitrogen concentrations of root and stem to leaves. η is a factor scaling live stem mass to LAI and tree height H . We adopt the same values of n_0 , n_{rl} , n_{wk} and η as that of TRIFFID model (Table 1) except that n_{rl} is set to 0.5 following observations of deciduous trees by Sugiura and Tateno (2011). The growth respiration is dependent on the residual between GPP and R_{am} based on a ratio r_g set to 0.2 for all PFTs (Knorr, 2000):

$$R_{ag} = r_g \cdot (GPP - R_{am}) \quad (24)$$

The λ in Equation (19) is a partitioning coefficient determining the fraction of NPP used for spreading:

$$\lambda = \begin{cases} 1, & \text{if } LAI_b > LAI_{\max} \\ \frac{LAI_b - LAI_{\min}}{LAI_{\max} - LAI_{\min}}, & \text{if } LAI_{\min} \leq LAI_b \leq LAI_{\max} \\ 0, & \text{if } LAI_b < LAI_{\min} \end{cases} \quad (25)$$

where LAI_{\min} and LAI_{\max} are minimum and maximum LAI values for a specific PFT (Table 1). In the current model version, we turn off the fractional changes by omitting λNPP in the carbon allocation but feeding it as input for the soil respiration. The litter fall rate Λ_l in Equation (19) consists of contributions from leaf, root, and stem as follows,

$$\Lambda_l = \gamma_l \cdot C_l + \gamma_r \cdot C_r + \gamma_w \cdot C_w \quad (26)$$

here γ_l , γ_r , and γ_w are turnover rate (yr^{-1}) for leaf, root, and stem carbon respectively. The leaf turnover rate is calculated based on the phenology change every day. The root and stem turnover rates are PFT-specific constants (Table 1), derived based on the meta-

Xu Yue 6/24/15 3:34 PM

Deleted: $N_w = n_{wl} \cdot n_0 \cdot C_w$

Unknown

Field Code Changed

Xu Yue 6/24/15 3:34 PM

Deleted: .

Xu Yue 6/24/15 3:34 PM

Formatted: Font:Italic

Xu Yue 6/24/15 3:34 PM

Deleted: n_{wl}

Xu Yue 6/24/15 3:34 PM

Formatted: Font:Not Italic

Xu Yue 6/24/15 3:34 PM

Deleted: vegetation type (Table 1).

Xu Yue 6/24/15 3:34 PM

Deleted: The root and stem turnover rates are PFT-specific constants (Table 1), derived based on the meta-analysis by Gill and Jackson (2000) for root and Houghton (2007)

analysis by Gill and Jackson (2000) for root and Stephenson and van Mantgem (2005) for stem.

3.4 Soil respiration

The soil respiration scheme is developed based on the Carnegie-Ames-Stanford Approach (CASA) model (Potter et al., 1993; Schaefer et al., 2008), which considers carbon flows among 12 biogeochemical pools. Three live pools, including leaf C_l , root C_r , and wood C_w , contain biomass carbon assimilated from photosynthesis. Litterfall from live pools decomposes and transits in nine dead pools, which consist of one coarse woody debris (CWD) pool, three surface pools, and five soil pools. The CWD pool is composed of dead trees and woody roots. Both surface and soil have identical pools, namely structural, metabolic, and microbial pools, which are distinguished by the content and functions. The structural pool contains lignin, the metabolic pool contains labile substrates, and the microbial pool represents microbial populations. The remaining two soil pools, the slow and passive pools, consist of organic material that decays slowly. The full list of carbon flows among different pools has been illustrated by Schaefer et al. (2008) (c.f. their Fig. 1).

When carbon transfers from pool j to pool i , the carbon loss of pool j is:

$$L_{j2i} = f_{j2i} k_j C_j \quad (27)$$

where C_j is the carbon in pool j , k_j is the total carbon loss rate of pool j , and f_{j2i} is the fraction of carbon lost from pool j transferred to pool i . The coefficient k_j is dependent on soil temperature, moisture, and texture. Meanwhile, the carbon gain of pool i is:

$$G_{j2i} = e_{j2i} \cdot L_{j2i} = e_{j2i} f_{j2i} k_j C_j \quad (28)$$

where e_{j2i} is the ratio of carbon received by pool i to the total carbon transferred from pool j . The rest of the transferred carbon is lost due to heterotrophic respiration:

Xu Yue 6/24/15 3:34 PM

Deleted: (Schaefer et al., 2008)

$$R_{j2i} = (1 - e_{j2i}) \cdot L_{j2i} \quad (29)$$

As a result, the carbon in the i th pool is calculated as

$$\frac{dC_i}{dt} = \sum_{j=1}^n G_{j2i} - \sum_{k=1}^m L_{i2k} \quad (30)$$

The total heterotrophic respiration (R_h) is the summation of R_{j2i} for all pair pools where carbon transitions occur. The total soil carbon is the summation of carbon for all dead pools:

$$C_{soil} = \sum_{i=1}^9 C_i \quad (31)$$

The net ecosystem productivity (NEP) is calculated as

$$NEP = -NEE = NPP - R_h = GPP - R_a - R_h \quad (32)$$

where NEE is the net ecosystem exchange, representing net carbon flow from land to atmosphere. YIBs does not yet account for NEE perturbations due to dynamic disturbance.

3.5 Ozone vegetation damage effects

We apply the semi-mechanistic parameterization proposed by Sitch et al. (2007) to account for ozone damage to photosynthesis through stomatal uptake. The scheme simulates associated changes in both photosynthetic rate and stomatal conductance. When photosynthesis is inhibited by ozone, stomatal conductance decreases accordingly to resist more ozone molecules. We employed an off-line regional version of YIBs to show that present-day ozone damage decreases GPP by 4-8% on average in the eastern U.S. and leads to larger decreases of 11-17% in east coast hotspots (Yue and Unger,

2014). In the current model version, the photosynthesis and stomatal conductance responses to ozone damage are coupled. In future work, we will update the ozone vegetation damage function in YIBs to account for decoupled photosynthesis and stomatal conductance responses based on recent extensive meta-data analyses (Wittig et al., 2007; Lombardozzi et al., 2013).

3.6 Biogenic volatile organic compound (BVOC) emissions

YIBs incorporates two independent leaf-level isoprene emission schemes embedded within the exact same host model framework (Zheng et al., 2015). The photosynthesis-based isoprene scheme simulates emission as a function of the electron transport-limited photosynthesis rate (J_e , Equation 3), canopy temperature, intercellular CO_2 (c_i) and Γ^* (Arneth et al., 2007; Unger et al., 2013). The MEGAN scheme applies the commonly used leaf-level functions of light and canopy temperature (Guenther et al., 1993; Guenther et al., 1995; Guenther et al., 2012). Both isoprene schemes account for atmospheric CO_2 -sensitivity (Arneth et al., 2007). Long-term increases (decreases) in atmospheric CO_2 decrease (increase) isoprene emissions (Unger et al., 2013). The CO_2 -sensitivity is higher under lower atmospheric CO_2 levels than present day. Leaf-level monoterpene emissions are simulated using a simplified temperature dependent algorithm (Lathiere et al., 2006). The leaf-level isoprene and monoterpene emissions are integrated over the multiple canopy layers in the exact same way as GPP to obtain the total canopy-level emissions.

3.7 Implementation of YIBs into NASA ModelE2 (NASA ModelE2-YIBs)

NASA ModelE2 has a spatial resolution of $2^\circ \times 2.5^\circ$ latitude by longitude with 40 vertical levels extending to 0.1 hPa. In the on-line configuration, the global climate model provides the meteorological drivers to YIBs and the land-surface hydrology submodel provides the soil characteristics (Rosenzweig and Abramopoulos, 1997; Schmidt et al., 2014). Recent relevant updates to NASA ModelE2 include a dynamic fire activity parameterization from Pechony and Shindell (2009) and climate-sensitive soil NO_x emissions based on Yienger and Levy (1995) (Unger and Yue, 2014). Without the YIBs implementation, the default NASA ModelE2 computes dry deposition using fixed LAI

Xu Yue 6/24/15 3:34 PM

Deleted: . Recent relevant updates to NASA ModelE2 include a dynamic fire activity parameterization from Pechony and Shindell (2009) and climate-sensitive soil NO_x emissions based on Yienger and Levy (1995) (Unger and Yue, 2014). Without the YIBs implementation, the default NASA ModelE2 computes dry deposition using fixed LAI and vegetation cover fields from Olson et al. (2001), which are different from the climate model's vegetation scheme. With YIBs embedded in NASA ModelE2, the YIBs model provides the vegetation cover and LAI for the dry deposition scheme. The on-line simulated atmospheric ozone and aerosol concentrations influence terrestrial carbon assimilation and stomatal conductance at the 30-minute integration time step. In turn, the on-line vegetation properties, and water, energy and BVOC fluxes affect air quality, meteorology and the atmospheric chemical composition. The model simulates the deposition of inorganic and organic nitrogen to the terrestrial biosphere. However, the YIBs biosphere currently applies fixed nitrogen levels and does not yet account for the dynamic interactions between the carbon and nitrogen cycles, and the consequences for carbon assimilation, which are highly uncertain (e.g., Thornton et al., 2007).

and vegetation cover fields from Olson et al. (2001), which are different from the climate model's vegetation scheme (Shindell et al., 2013b). With YIBs embedded in NASA ModelE2, the YIBs model provides the vegetation cover and LAI for the dry deposition scheme. The on-line simulated atmospheric ozone and aerosol concentrations influence terrestrial carbon assimilation and stomatal conductance at the 30-minute integration time step. In turn, the on-line vegetation properties, and water, energy and BVOC fluxes affect air quality, meteorology and the atmospheric chemical composition. The model simulates the interactive deposition of inorganic and organic nitrogen to the terrestrial biosphere. However, the YIBs biosphere currently applies fixed nitrogen levels and does not yet account for the dynamic interactions between the carbon and nitrogen cycles, and the consequences for carbon assimilation, which are highly uncertain (e.g., Thornton et al., 2007; Koven et al., 2013; Thomas et al., 2013; Zaehle et al., 2014; Houlton et al., 2015).

4. Model setup and simulations

4.1 Site-level simulations (YIBs-site)

We perform site-level simulations with offline YIBs model at 145 eddy covariance flux tower sites for the corresponding PFTs (Fig. 1). Hourly *in situ* measurements of meteorology (Sect. 2.1) are used as input for the model. We gap filled missing measurements with the Global Modeling and Assimilation Office (GMAO) Modern Era-Retrospective Analysis (MERRA) reanalysis (Rienecker et al., 2011), as described in Yue and Unger (2014). All grasslands and most croplands are considered as C3 plants, except for some sites where corn is grown. Meteorological measurements are available for a wide range of time periods across the different sites ranging from the minimum of 1 year at some sites (e.g. BE-Jal) and the maximum of 16 years at Harvard Forest (US-HA1). The soil carbon pool initial conditions at each site are provided by the 140-year spin up procedure using YIBs-offline (Supplement). An additional 30-year spin up is conducted for each site-level simulation using the initial height H_0 for corresponding PFT (Table 1) and the fixed meteorology and CO₂ conditions at the first year of observations. Then, the simulation is continued with year-to-year forcings at the specific site for the rest of measurement period. For all grass and shrub sites, two simulations are performed. One

Xu Yue 6/24/15 3:34 PM

Deleted: .

Xu Yue 6/24/15 3:34 PM

Deleted: section

Xu Yue 6/24/15 3:34 PM

Deleted: For

Xu Yue 6/24/15 3:34 PM

Deleted: , we

Xu Yue 6/24/15 3:34 PM

Deleted: the

Xu Yue 6/24/15 3:34 PM

Deleted: model

Xu Yue 6/24/15 3:34 PM

Deleted: 30 years with

Xu Yue 6/24/15 3:34 PM

Deleted: concentrations

Xu Yue 6/24/15 3:34 PM

Deleted: , and then continue simulations

Xu Yue 6/24/15 3:34 PM

Deleted: observations

Xu Yue 6/24/15 3:34 PM

Deleted: same

Xu Yue 6/24/15 3:34 PM

Deleted: observation

659 | applies additional drought controls on phenology as described in [Sects. 3.2.2 and 3.2.3](#),
 660 | while the other uses only temperature-dependent phenology. By comparing results of
 661 | these two simulations, we assess the role of drought phenology for plants in arid and
 662 | semi-arid regions.

663

664 | 4.2 Global off-line simulation (YIBs-offline)

665 | The global off-line YIBs applies the CLM land cover dataset (Oleson et al., 2010). Land
 666 | cover is derived based on retrievals from both MODIS (Hansen et al., 2003) and AVHRR
 667 | (Defries et al., 2000). Fractions of 16 PFTs are aggregated into 9 model PFTs (Table 1).
 668 | [The soil carbon pool and tree height initial conditions are provided by the 140-year spin](#)
 669 | [up procedure using YIBs-offline \(Supplement\).](#) The global off-line YIBs model is driven
 670 | with WFDEI meteorology (Weedon et al., 2014) at $1^\circ \times 1^\circ$ horizontal resolution for the
 671 | period of 1980-2011. [Observed atmospheric CO₂ concentrations](#) are adopted from the
 672 | fifth assessment report (AR5) of the Intergovernmental Panel on Climate Change (IPCC)
 673 | (Meinshausen et al., 2011). We evaluate the simulated long-term [1980-2011](#) average tree
 674 | height/LAI and carbon fluxes with available observations and recent multi-model inter-
 675 | comparisons. Attribution of the decadal trends in terrestrial carbon fluxes are explored in
 676 | a separate follow-on companion study (Yue et al., 2015b).

677

678 | 4.3 Global on-line simulation in NASA ModelE2-YIBs

679 | The global land cover data is identical to that used in YIBs-offline ([Sect. 4.2](#)) based on
 680 | the CLM cover. Because our major research goal is to study short-term (seasonal, annual,
 681 | decadal) interactions between vegetation physiology and atmospheric chemistry, we elect
 682 | to prescribe the PFT distribution in different climatic states. We perform an on-line
 683 | atmosphere-only simulation representative of the present day (~2000s) climatology by
 684 | prescribing fixed monthly-average sea surface temperature (SST) and sea ice temperature
 685 | for the 1996-2005 decade from the Hadley Center as the boundary conditions (Rayner et
 686 | al., 2006). Atmospheric CO₂ concentration is fixed at the level of the year 2000 (370
 687 | ppm). [In NASA ModelE2-YIBs, initial conditions for soil carbon pools and tree heights](#)
 688 | [are provided by the 140-year spin-up process described in the Supplement using YIBs-](#)
 689 | [offline but for year 2000 \(not 1980\) fixed WFDEI meteorology and atmospheric CO₂](#)

Xu Yue 6/24/15 3:34 PM

Deleted: sections

Xu Yue 6/24/15 3:34 PM

Deleted: Tree height and soil carbon pools from the spin-up process (Supporting Information) are used as initial conditions.

Unknown

Field Code Changed

Xu Yue 6/24/15 3:34 PM

Deleted: section

Xu Yue 6/24/15 3:34 PM

Deleted: The

Xu Yue 6/24/15 3:34 PM

Deleted: supporting information

Xu Yue 6/24/15 3:34 PM

Deleted: the off-line YIBs model is repeated

Xu Yue 6/24/15 3:34 PM

Deleted: with

Xu Yue 6/24/15 3:34 PM

Deleted: [

Xu Yue 6/24/15 3:34 PM

Deleted:] at the year 2000 values. We use the derived tree height and soil pools as initial

conditions. The NASA ModelE2-YIBs global carbon-chemistry-climate model is run for an additional 30 model years. The first 20 years are discarded as the on-line spin-up and the last 10-year results are averaged for the analyses including comparisons with observations and the YIBs-offline.

4.4 Ozone vegetation damage simulation (YIBs-ozone)

We perform two simulations to quantify ozone vegetation damage with the off-line YIBs model based on the high and low ozone sensitivity parameterizations (Sitch et al., 2007). Similar to the set up in Yue and Unger (2014), we use off-line hourly surface ozone concentrations simulated with the NASA ModelE2 based on the climatology and precursor emissions of the year 2000 (Sect. 4.3). In this way, atmospheric ozone photosynthesis damage affects plant growth, including changes in tree height and LAI. We compare the simulated ozone damage effects with the previous results in Yue and Unger (2014) that used prescribed LAI. For this updated assessment, we do not isolate possible feedbacks from the resultant land carbon cycle changes to the surface ozone concentrations themselves, for instance through concomitant changes to BVOC emissions and water fluxes. The importance of these feedbacks will be quantified in future research using the on-line NASA ModelE2-YIBs framework.

5. Results

5.1 Site-level evaluation

The simulated monthly-average GPP is compared with measurements at 145 sites for different PFTs (Fig. 3). GPP simulation biases range from -19% to 7% depending on PFT. The highest correlation of 0.86 is achieved for DBF, mainly contributed by the reasonable phenology simulated at these sites (Fig. S2). The correlation is also high for ENF sites even though phenology is set to a constant value of 1.0. A relatively low correlation of 0.65 is modeled for EBF sites (Fig. S2). However, the site-specific evaluation shows that the simulations reasonably capture the observed magnitude and seasonality, including the minimum GPP in summer due to drought at some sites (e.g. FR-Pue and IT-Lec). Predictions at crop sites achieve a medium correlation of 0.77,

Xu Yue 6/24/15 3:34 PM

Deleted: for the on-line

Xu Yue 6/24/15 3:34 PM

Deleted: present-day simulation and

Xu Yue 6/24/15 3:34 PM

Deleted: section

Xu Yue 6/24/15 3:34 PM

Deleted: , because the inhibition of V_{cmax} by frost hardening captures the observed low GPP in cold seasons

739 because the prescribed crop phenology based on the planting and harvesting dates dataset
740 matches reality for most sites with some exceptions (e.g. CH-Oe2). Measured GPP at
741 shrub and grass sites show varied seasonality. For most sites, the maximum carbon fluxes
742 are measured in the hemispheric summer season. However, for sites with arid or
743 Mediterranean climate, the summer GPP is usually the lowest during the year (e.g. ES-
744 LMa and US-Var in Fig. S2) while the peak flux is observed during the wet season when
745 the climate is cooler and moister. Implementing the drought-dependent phenology helps
746 improve the GPP seasonality and decrease the root-mean-square error (RMSE) at most
747 warm climate shrub and grass sites (Fig. S3).

748
749 A synthesis of the site-level evaluation is presented in Fig. 4. Among the 145 sites, 121
750 have correlations higher than 0.8 for the GPP simulation (Fig. 4a). Predictions are better
751 for PFTs with larger seasonal variations. For example, high correlations of >0.8 are
752 achieved at 95% ENF and DBF sites, but only 70% for grass and 45% for EBF sites. Low
753 relative biases (-33%-50%) are achieved at 94 sites (Fig. 4b). For most PFTs, a similar
754 fraction (65%) of the sites have low biases falling into that range, except for cropland,
755 where only 7 sites (45%) have the low biases. The RMSE is lower than 3 g [C] day⁻¹ for
756 107 out of 145 sites (Fig. 4c). The highest RMSE is predicted for crop sites, where the
757 model misses the large interannual variations due to crop rotation at some sites (e.g. BE-
758 Lon, DE-Geb, and US-Ne2). YIBs model performs simulations at the PFT level while
759 measurements show large uncertainties in the carbon fluxes among biomes/species within
760 the same PFT (Luyssaert et al., 2007). The simulated intraspecific variations (in the form
761 of standard deviation) are smaller than the measured/derived values for most PFTs (Table
762 S2), likely because of the application of fixed photosynthetic parameters for each PFT
763 (Table 1).

764
765 Compared with GPP, the NEE simulations have smaller correlations with measurements
766 because of the limited seasonality in the observations at most sites (Fig. S4). 74 sites
767 (51%) have correlation coefficients higher than 0.6 (Fig. 4d) and 75 sites (52%) have
768 absolute biases within ± 0.5 g [C] day⁻¹ (Fig. 4e). For most ENF sites, the maximum net
769 carbon uptake (the minimum NEE) is observed in spring or early summer, when GPP

Xu Yue 6/24/15 3:34 PM

Deleted: 4c

Xu Yue 6/24/15 3:34 PM

Deleted: 4e

Xu Yue 6/24/15 3:34 PM

Deleted: 4b

Xu Yue 6/24/15 3:34 PM

Deleted: 4d

begins to increase while soil respiration is still at low rate due to the cool and wet conditions (e.g. CA-Ojp and ES-ES1). Compared with other PFTs, the DBF trees usually have larger seasonality with the NEE peak in the early summer. Such seasonality helps promote correlations between model and measurements, resulting in high R (>0.8) for 17 out of 20 sites (Fig. 4d). For shrub and grass sites, the observed seasonality of NEE is not regular, though most show maximum carbon uptake in spring or early summer. Implementation of drought-dependent phenology helps improve the simulated NEE seasonality at some sites of these PFTs (e.g. ES-LMa and IT-Pia), however, such improvement is limited for others (Fig. S4). Simulated crop NEE reaches maximum magnitude in summer at most sites, consistent with observations and leading to a high R (> 0.8) for 10 out 16 sites (Fig. 4d). The RMSE of simulated NEE is larger for crop relative to other PFTs because the model does not treat crop rotation (Fig. 4f).

5.2 Evaluation of YIBs-offline

YIBs-offline forced with WFDEI meteorology simulates reasonable spatial distributions for tree height, LAI, and GPP, all of which show maximums in the tropical rainforest biome and medium values in the Northern Hemisphere high latitudes (Fig. 5). Compared with the satellite observations, the simulated height is underestimated by 30% on the annual and global mean basis (Fig. 5b). Regionally, the prediction is larger by only 4% for tropical rainforest and temperate DBF, but by 27% for boreal ENF, for which the model assumes a constant phenology of 1.0 all the year round. However, for the vast areas covered with grass and shrub PFTs, the simulated height is lower by 41% with maximum underestimation in Eastern Siberia, where the model land is covered by short tundra. The modeled LAI is remarkably close to observations on the annual and global mean basis (Figs. 5c-d). However, there are substantial regional biases in model LAI. Model LAI prediction is higher by $0.8 \text{ m}^2 \text{ m}^{-2}$ (70%) for boreal ENF and by $0.1 \text{ m}^2 \text{ m}^{-2}$ (5%) for tropical rainforest. In contrast, the simulation underestimates LAI of tropical C4 grass by $0.4 \text{ m}^2 \text{ m}^{-2}$ (30%) and shrubland by $0.2 \text{ m}^2 \text{ m}^{-2}$ (30%). The GPP simulation is lower than the FLUXNET-derived value by 5% on the global scale, which is contributed by the minor underestimation for all PFTs except for tropical rainforest, where model predicts 9% higher GPP than observations (Fig. 5f).

Xu Yue 6/24/15 3:34 PM

Deleted: 4b

Xu Yue 6/24/15 3:34 PM

Deleted: 4b

807

808 The model simulates reasonable seasonality for LAI and land carbon fluxes (Fig. 6). Tree
809 height shows limited seasonal variations, especially for DBF, ENF, and EBF trees. LAI,
810 GPP, and NPP also exhibit small seasonality over tropical areas, such as the Amazon,
811 Central Africa, and Indonesia. However, for temperate areas, such as North America,
812 Europe and East Asia, these variables show large seasonal variations with minimum in
813 winter and maximum in summer. The LAI is overestimated by 20% in Amazon during
814 the December-January-February season but underestimated by 25% in Indonesia during
815 summer (Fig. 6b). For GPP and NPP, the positive bias in Indonesia is even larger at 45%
816 during summer (Figs. 6c-d).

817

818 On the global scale, YIBs-offline simulates GPP of $124.6 \pm 3.3 \text{ Pg C a}^{-1}$ and NEE of -2.5
819 $\pm 0.7 \text{ Pg C a}^{-1}$ for 1982-2011. These values are consistent with estimates upscaled from
820 the FLUXNET observations (Jung et al., 2009; Friedlingstein et al., 2010; Jung et al.,
821 2011) and simulations from 10 other carbon cycle models (Piao et al., 2013) (Fig. 7). The
822 net biome productivity (NBP) is in opposite sign to NEE. Tropical areas (23°S-23°N)
823 account for 63% of the global GPP, including 27% from Amazon rainforest, 21% from
824 central Africa, and 5% from Indonesia forest (Table 3). A lower contribution of 57%
825 from tropics is predicted for both NPP and heterotrophic respiration. However, for NEE,
826 only 40% of the land carbon sink is contributed by tropical forests and grasslands, while
827 56% is from temperate forests and grasslands in North America, Europe, and East Asia. ▼

828

829 We compare the simulated budburst dates with observations from satellite retrieval (Fig.
830 8). The model captures the basic spatial pattern of spring phenology with earlier to later
831 budburst dates from lower to higher latitudes. On average, the observed budburst date in
832 Northern Hemisphere (NH) is 133 DOY (May 13th) and simulation is 132 DOY (May
833 12th). Such close estimate results from the regional delay of 10 days (119 versus 129
834 DOY) in Europe and advance of 4 days (140 versus 136 DOY) in East Asia. In Y2015,
835 extensive (~75000 records) ground-based measurements have been used to validate the
836 simulated spring and autumn phenology in U.S. and both the spatial distribution and
837 interannual variation of simulation are reasonable.

Xu Yue 6/24/15 3:34 PM

Deleted: 53

Xu Yue 6/24/15 3:34 PM

Deleted: 46

Xu Yue 6/24/15 3:34 PM

Deleted: 32

Xu Yue 6/24/15 3:34 PM

Deleted: The NEE differences between the tropical and temperate biomes are largely driven by the higher dark respiration rate and enhanced autotrophic respiration in the warmer climate zone.

5.3 Evaluation of NASA ModelE2-YIBs

NASA ModelE2-YIBs simulations of global land carbon fluxes show similar spatial distribution and magnitude as the YIBs-offline model (Figs. S6-S8). However, due to differences in the meteorological forcings (Figs. S9-S12), regional discrepancies between the two configurations occur. The predicted LAI with NASA ModelE2-YIBs is lower by 20% in Amazon region than YIBs-offline (Fig. S6), following the similar magnitude of differences in regional GPP and NPP (Figs. S7-S8). We performed driver attribution sensitivity simulations, in which the YIBs-offline configuration is driven with the same meteorological forcings simulated by NASA ModelE2 except for one selected field from the WFDEI reanalysis. We found that the anomalously warmer climate over the Amazon in the global climate model (Fig. S9) causes the lower GPP in that region in NASA ModelE2-YIBs. The temperature optimum for C3 photosynthesis is around 30 °C, above which the maximum rate of electron transport (Equation 3) decreases dramatically (Farquhar et al., 1980). As a result, the higher NASA ModelE2-YIBs surface temperature in the tropical rainforest results in the lower photosynthesis rates there. With the exception of the Amazon, the NASA ModelE2-YIBs June-July-August GPP and NPP show low biases in central Africa and high latitudes in North America and Asia, but high biases in Europe, western U.S., and eastern China (Figs. S7-S8). The sensitivity tests attribute these discrepancies to differences in canopy humidity (Fig. S11) and soil wetness (Fig. S12). Low soil wetness decreases water stress β , reduces the slope m of Ball-Berry equation (Equation 6), and consequently limits photosynthesis by declining stomatal conductance in combination with low humidity. On the global scale, the ModelE2-YIBs simulates annual GPP of 122.9 Pg C, NPP of 62 Pg C, and NEE of -2.7 Pg C, all of which are close to the YIBs-offline simulation (Table 3) and consistent with results from observations and model inter-comparison (Fig. 7).

5.4 Assessment of global ozone vegetation damage

Ozone dampens GPP and consequently affects tree growth and LAI. In North America, the annual average reductions range from 2% to 6%, depending on the plant sensitivity to

ozone damage (Table 3). Locally, average damages reach as high as 5-11% in the eastern U.S. with maximums up to 11-23% (Figs. 9a-b). These values are higher than the estimate of 4-8% (maximum 11-17%) by Yue and Unger (2014), because the latter used prescribed LAI in the simulation and did not consider the LAI reductions due to ozone damage (Figs. 9c-d). The YIBs model predicts similar magnitude of damages in Europe compared to North America, but almost doubled effects in East Asia (Table 3) due to the high ozone concentrations there, especially in boreal summer (Fig. S5). Ozone-induced GPP-reductions are limited in tropical areas (Fig. 5e) because the surface ozone levels there are very low, for example, especially over the Amazon forest (Fig. S5). The damage to LAI generally follows the pattern of GPP reductions but the response signal is weaker than that of GPP (Figs. 9c-d).

6. Conclusions and discussion

We describe and evaluate the process-based YIBs interactive terrestrial biosphere model. YIBs is embedded into the NASA ModelE2 global chemistry-climate model and is an important urgently needed development to improve the biological realism of interactions between vegetation, atmospheric chemistry and climate. We implement both temperature- and drought-dependent phenology for DBF, shrub, and grass species. The model simulates interactive ozone vegetation damage. The YIBs model is fully validated with land carbon flux measurements from 145 ground stations and global observations of canopy height, LAI, GPP, NPP, and phenology from multiple satellite retrievals.

There are several limitations in the current model set up. The vegetation parameters, V_{cmax25} , m , and b (Table 1), are fixed at the PFT level, which may induce uncertainties in the simulation of carbon fluxes due to intraspecific variations (Kattge et al., 2011). The model does not yet include a dynamic treatment of nitrogen and phosphorous availability because current schemes suffer from large uncertainties (Thornton et al., 2007; Zaehle et al., 2014; Houlton et al., 2015). Phenology is set to a constant value of 1 for ENF and EBF, which is not consistent with observations (O'Keefe, 2000; Jones et al., 2014). The ozone damage scheme of Sitch et al. (2007) considers coupled responses of

Xu Yue 6/24/15 3:34 PM

Deleted: not well calibrated for

Xu Yue 6/24/15 3:34 PM

Deleted: tropical rainforest biome

Xu Yue 6/24/15 3:34 PM

Deleted: the limited availability of tropical site measurement data (Fig. 1).

Xu Yue 6/24/15 3:34 PM

Deleted: (Thornton et al., 2007; Zaehle et al., 2014)

914 photosynthesis and stomatal conductance while observations suggest a decoupling
915 (Lombardozzi et al., 2013).

916
917 Despite these limitations, the YIBs model reasonably simulates global land carbon fluxes
918 compared with both site-level flux measurements and global satellite observations. YIBs
919 is primed for on-going development, for example, incorporating community dynamics
920 including mortality, establishment, seed transport and dynamic fire disturbance
921 (Moorcroft et al., 2001). NASA ModelE2-YIBs is available to be integrated with
922 interactive ocean and atmospheric carbon components to offer a full global carbon-
923 climate model, for example for use in interpreting and diagnosing new satellite datasets
924 of atmospheric CO₂ concentrations. In the current form, NASA ModelE2-YIBs provides
925 a useful new tool to investigate the impacts of air pollution on the carbon budget, water
926 cycle, and surface energy balance, and, in turn, the impacts of changing vegetation
927 physiology on the atmospheric chemical composition. Carbon-chemistry-climate
928 interactions, a relatively new interdisciplinary research frontier, are expected to influence
929 the evolution of the Earth's climate system on multiple spatiotemporal scales.

931 Code availability

932
933 The YIBs model (version 1.0) site-level source code is available at
934 https://github.com/YIBS01/YIBS_site. The source codes for the global off-line and
935 global on-line versions of the YIBs model (version 1.0) are available through
936 collaboration. Please submit request to X. Yue (xu.yue@yale.edu) and N. Unger
937 (nadine.unger@yale.edu). Auxiliary forcing data and related input files must be obtained
938 independently.

939
940 *Acknowledgements.* Funding support for this research is provided by the NASA
941 Atmospheric Composition Campaign Data Analysis and Modeling Program. This project
942 was supported in part by the facilities and staff of the Yale University Faculty of Arts and
943 Sciences High Performance Computing Center. The authors would like to thank Ranga B.
944 Myneni and Zaichun Zhu for providing the AVHRR LAI3g dataset.

Xu Yue 6/24/15 3:34 PM
Formatted: Space After: 0 pt

Xu Yue 6/24/15 3:34 PM
Formatted: Font: Times New Roman

References

- Ainsworth, E. A., Yendrek, C. R., Sitch, S., Collins, W. J., and Emberson, L. D.: The effects of tropospheric ozone on net primary productivity and implications for climate change, *Annu Rev Plant Biol*, 63, 637-661, doi:10.1146/Annurev-Arplant-042110-103829, 2012.
- Arneth, A., Niinemets, U., Pressley, S., Back, J., Hari, P., Karl, T., Noe, S., Prentice, I. C., Serca, D., Hickler, T., Wolf, A., and Smith, B.: Process-based estimates of terrestrial ecosystem isoprene emissions: incorporating the effects of a direct CO₂-isoprene interaction, *Atmos Chem Phys*, 7, 31-53, doi:10.5194/acp-7-31-2007, 2007.
- Baldocchi, D.: An Analytical Solution for Coupled Leaf Photosynthesis and Stomatal Conductance Models, *Tree Physiol*, 14, 1069-1079, 1994.
- Ball, J. T., Woodrow, I. E., and Berry, J. A.: A model predicting stomatal conductance and its contribution to the control of photosynthesis under different environmental conditions. In: *Progress in Photosynthesis Research*, Biggins, J. (Ed.), Nijhoff, Dordrecht, Netherlands, 1987.
- Beer, C., Reichstein, M., Tomelleri, E., Ciais, P., Jung, M., Carvalhais, N., Rodenbeck, C., Arain, M. A., Baldocchi, D., Bonan, G. B., Bondeau, A., Cescatti, A., Lasslop, G., Lindroth, A., Lomas, M., Luyssaert, S., Margolis, H., Oleson, K. W., Rouspard, O., Veenendaal, E., Viovy, N., Williams, C., Woodward, F. I., and Papale, D.: Terrestrial Gross Carbon Dioxide Uptake: Global Distribution and Covariation with Climate, *Science*, 329, 834-838, doi:10.1126/Science.1184984, 2010.
- Berry, J. A., Beerling, D. J., and Franks, P. J.: Stomata: key players in the earth system, past and present, *Curr Opin Plant Biol*, 13, 233-240, doi:10.1016/J.Pbi.2010.04.013, 2010.
- Bonan, G. B., Lawrence, P. J., Oleson, K. W., Levis, S., Jung, M., Reichstein, M., Lawrence, D. M., and Swenson, S. C.: Improving canopy processes in the Community Land Model version 4 (CLM4) using global flux fields empirically inferred from FLUXNET data, *J. Geophys. Res.*, 116, G02014, doi:10.1029/2010jg001593, 2011.
- Bonan, G. B., Levis, S., Sitch, S., Vertenstein, M., and Oleson, K. W.: A dynamic global vegetation model for use with climate models: concepts and description of simulated vegetation dynamics, *Global Change Biol*, 9, 1543-1566, doi:10.1046/J.1365-2486.2003.00681.X, 2003.
- Clark, D. B., Mercado, L. M., Sitch, S., Jones, C. D., Gedney, N., Best, M. J., Pryor, M., Rooney, G. G., Essery, R. L. H., Blyth, E., Boucher, O., Harding, R. J., Huntingford, C., and Cox, P. M.: The Joint UK Land Environment Simulator (JULES), model description - Part 2: Carbon fluxes and vegetation dynamics, *Geosci Model Dev*, 4, 701-722, doi:10.5194/Gmd-4-701-2011, 2011.
- Collatz, G. J., Ball, J. T., Grivet, C., and Berry, J. A.: Physiological and Environmental Regulation of Stomatal Conductance, Photosynthesis and Transpiration - a Model That Includes a Laminar Boundary-Layer, *Agr Forest Meteorol*, 54, 107-136, doi:10.1016/0168-1923(91)90002-8, 1991.
- Collatz, G. J., Ribas-Carbo, M., and Berry, J. A.: Coupled Photosynthesis-Stomatal Conductance Model for Leaves of C₄ Plants, *Aust J Plant Physiol*, 19, 519-538, 1992.
- Cox, P. M.: Description of the "TRIFFID" Dynamic Global Vegetation Model, Hadley Centre technical note 24, 2001.

Xu Yue 6/24/15 3:34 PM

Deleted: Page Break

Xu Yue 6/24/15 3:34 PM

Formatted: Indent: Left: 0", Hanging: 0.25"

Xu Yue 6/24/15 3:34 PM

Deleted: C.R.

Xu Yue 6/24/15 3:34 PM

Deleted: S.

Xu Yue 6/24/15 3:34 PM

Formatted: EndNote Bibliography, Left

Xu Yue 6/24/15 3:34 PM

Deleted: W.J.

Xu Yue 6/24/15 3:34 PM

Deleted: L.D.

Xu Yue 6/24/15 3:34 PM

Deleted: :

Xu Yue 6/24/15 3:34 PM

Deleted: Annual Review of

Xu Yue 6/24/15 3:34 PM

Deleted: Biology

Xu Yue 6/24/15 3:34 PM

Formatted: EndNote Bibliography, Left

Xu Yue 6/24/15 3:34 PM

Formatted: EndNote Bibliography, Left

Xu Yue 6/24/15 3:34 PM

Formatted: EndNote Bibliography, Left

1000 | Defries, R. S., Hansen, M. C., Townshend, J. R. G., Janetos, A. C., and Loveland, T. R.:
1001 | A new global 1-km dataset of percentage tree cover derived from remote sensing,
1002 | *Global Change Biol*, 6, 247-254, doi:10.1046/J.1365-2486.2000.00296.X, 2000.

1003 | Delbart, N. and Picard, G.: Modeling the date of leaf appearance in low-arctic tundra,
1004 | *Global Change Biol*, 13, 2551-2562, doi:10.1111/J.1365-2486.2007.01466.X, 2007.

1005 | Delpierre, N., Dufrene, E., Soudani, K., Ulrich, E., Cecchini, S., Boe, J., and Francois, C.:
1006 | Modelling interannual and spatial variability of leaf senescence for three deciduous
1007 | tree species in France, *Agr Forest Meteorol*, 149, 938-948,
1008 | doi:10.1016/J.Agrformet.2008.11.014, 2009.

1009 | Doughty, C. E. and Goulden, M. L.: Seasonal patterns of tropical forest leaf area index
1010 | and CO₂ exchange, *J. Geophys. Res.*, 113, G00b06, doi:10.1029/2007jg000590,
1011 | 2008.

1012 | Dufrene, E., Davi, H., Francois, C., le Maire, G., Le Dantec, V., and Granier, A.:
1013 | Modelling carbon and water cycles in a beech forest Part I: Model description and
1014 | uncertainty analysis on modelled NEE, *Ecol Model*, 185, 407-436,
1015 | doi:10.1016/J.Ecolmodel.2005.01.004, 2005.

1016 | Farquhar, G. D., Caemmerer, S. V., and Berry, J. A.: A Biochemical-Model of
1017 | Photosynthetic CO₂ Assimilation in Leaves of C-3 Species, *Planta*, 149, 78-90,
1018 | doi:10.1007/Bf00386231, 1980.

1019 | Friedlingstein, P., Andrew, R. M., Rogelj, J., Peters, G. P., Canadell, J. G., Knutti, R.,
1020 | Luderer, G., Raupach, M. R., Schaeffer, M., van Vuuren, D. P., and Le Quere, C.:
1021 | Persistent growth of CO₂ emissions and implications for reaching climate targets, *Nat*
1022 | *Geosci*, 7, 709-715, doi:10.1038/Ngeo2248, 2014.

1023 | Friedlingstein, P., Cox, P., Betts, R., Bopp, L., Von Bloh, W., Brovkin, V., Cadule, P.,
1024 | Doney, S., Eby, M., Fung, I., Bala, G., John, J., Jones, C., Joos, F., Kato, T.,
1025 | Kawamiya, M., Knorr, W., Lindsay, K., Matthews, H. D., Raddatz, T., Rayner, P.,
1026 | Reick, C., Roeckner, E., Schnitzler, K. G., Schnur, R., Strassmann, K., Weaver, A. J.,
1027 | Yoshikawa, C., and Zeng, N.: Climate-carbon cycle feedback analysis: Results from
1028 | the (CMIP)-M-4 model intercomparison, *J Climate*, 19, 3337-3353,
1029 | doi:10.1175/Jcli3800.1, 2006.

1030 | Friedlingstein, P., Houghton, R. A., Marland, G., Hackler, J., Boden, T. A., Conway, T.
1031 | J., Canadell, J. G., Raupach, M. R., Ciais, P., and Le Quere, C.: Update on CO₂
1032 | emissions, *Nat Geosci*, 3, 811-812, doi:10.1038/Ngeo1022, 2010.

1033 | Friend, A. D. and Kiang, N. Y.: Land surface model development for the GISS GCM:
1034 | Effects of improved canopy physiology on simulated climate, *J Climate*, 18, 2883-
1035 | 2902, doi:10.1175/Jcli3425.1, 2005.

1036 | Gill, R. A. and Jackson, R. B.: Global patterns of root turnover for terrestrial ecosystems,
1037 | *New Phytol*, 147, 13-31, doi:10.1046/J.1469-8137.2000.00681.X, 2000.

1038 | Guenther, A. B., Hewitt, C. N., Erickson, D., Fall, R., Geron, C., Graedel, T., Harley, P.,
1039 | Klinger, L., Lerdau, M., McKay, W. A., Pierce, T., Scholes, B., Steinbrecher, R.,
1040 | Tallamraju, R., Taylor, J., and Zimmerman, P.: A Global-Model of Natural Volatile
1041 | Organic-Compound Emissions, *J. Geophys. Res.*, 100, 8873-8892,
1042 | doi:10.1029/94jd02950, 1995.

1043 | Guenther, A. B., Jiang, X., Heald, C. L., Sakulyanontvittaya, T., Duhl, T., Emmons, L.
1044 | K., and Wang, X.: The Model of Emissions of Gases and Aerosols from Nature

version 2.1 (MEGAN2.1): an extended and updated framework for modeling biogenic emissions, *Geosci Model Dev*, 5, 1471-1492, doi:10.5194/Gmd-5-1471-2012, 2012.

Guenther, A. B., Zimmerman, P. R., Harley, P. C., Monson, R. K., and Fall, R.: Isoprene and Monoterpene Emission Rate Variability - Model Evaluations and Sensitivity Analyses, *J. Geophys. Res.*, 98, 12609-12617, doi:10.1029/93jd00527, 1993.

Hanninen, H. and Kramer, K.: A framework for modelling the annual cycle of trees in boreal and temperate regions, *Silva Fenn*, 41, 167-205, 2007.

Hansen, M. C., DeFries, R. S., Townshend, J. R. G., Carroll, M., Dimiceli, C., and Sohlberg, R. A.: Global Percent Tree Cover at a Spatial Resolution of 500 Meters: First Results of the MODIS Vegetation Continuous Fields Algorithm, *Earth Interact*, 7, 1-15, doi:10.1175/1087-3562(2003)007<0001:GPTCAA>2.0.CO;2, 2003.

Hollaway, M. J., Arnold, S. R., Challinor, A. J., and Emberson, L. D.: Intercontinental trans-boundary contributions to ozone-induced crop yield losses in the Northern Hemisphere, *Biogeosciences*, 9, 271-292, doi:10.5194/Bg-9-271-2012, 2012.

Houghton, R. A., House, J. I., Pongratz, J., van der Werf, G. R., DeFries, R. S., Hansen, M. C., Le Quere, C., and Ramankutty, N.: Carbon emissions from land use and land-cover change, *Biogeosciences*, 9, 5125-5142, doi:10.5194/Bg-9-5125-2012, 2012.

Houlton, B. Z., Marklein, A. R., and Bai, E.: Representation of nitrogen in climate change forecasts, *Nat Clim Change*, 5, 398-401, 2015.

Huntingford, C., Cox, P. M., Mercado, L. M., Sitch, S., Bellouin, N., Boucher, O., and Gedney, N.: Highly contrasting effects of different climate forcing agents on terrestrial ecosystem services, *Philos T R Soc A*, 369, 2026-2037, doi:10.1098/Rsta.2010.0314, 2011.

Jones, M. O., Kimball, J. S., and Nemani, R. R.: Asynchronous Amazon forest canopy phenology indicates adaptation to both water and light availability, *Environ Res Lett*, 9, 124021, doi:10.1088/1748-9326/9/12/124021, 2014.

Jung, M., Reichstein, M., and Bondeau, A.: Towards global empirical upscaling of FLUXNET eddy covariance observations: validation of a model tree ensemble approach using a biosphere model, *Biogeosciences*, 6, 2001-2013, doi:10.5194/bg-6-2001-2009, 2009.

Jung, M., Reichstein, M., Margolis, H. A., Cescatti, A., Richardson, A. D., Arain, M. A., Arneth, A., Bernhofer, C., Bonal, D., Chen, J. Q., Gianelle, D., Gobron, N., Kiely, G., Kutsch, W., Lasslop, G., Law, B. E., Lindroth, A., Merbold, L., Montagnani, L., Moors, E. J., Papale, D., Sottocornola, M., Vaccari, F., and Williams, C.: Global patterns of land-atmosphere fluxes of carbon dioxide, latent heat, and sensible heat derived from eddy covariance, satellite, and meteorological observations, *J. Geophys. Res.*, 116, G00j07, doi:10.1029/2010jg001566, 2011.

Kattge, J. and co-authors: TRY - a global database of plant traits, *Global Change Biol*, 17, 2905-2935, doi:10.1111/J.1365-2486.2011.02451.X, 2011.

Keenan, T. F., Gray, J., Friedl, M. A., Toomey, M., Bohrer, G., Hollinger, D. Y., Munger, J. W., O'Keefe, J., Schmid, H. P., SueWing, I., Yang, B., and Richardson, A. D.: Net carbon uptake has increased through warming-induced changes in temperate forest phenology, *Nat Clim Change*, 4, 598-604, doi:10.1038/Nclimate2253, 2014.

Kim, Y. and Wang, G. L.: Modeling seasonal vegetation variation and its validation against Moderate Resolution Imaging spectroradiometer (MODIS) observations over North America, *J. Geophys. Res.*, 110, D04106, doi:10.1029/2004jd005436, 2005.

Xu Yue 6/24/15 3:34 PM

Deleted: .. Balancing the global carbon budget, *Annu Rev Earth Pl Sc*, 35, 313-347, doi:10.1146/Annurev.Earth.35.031306.140057, 2007

Xu Yue 6/24/15 3:34 PM

Deleted: Houghton, R. A., House, J. I., Pongratz, J., van der Werf, G. R., DeFries, R. S., Hansen, M. C., Le Quere, C., and Ramankutty, N.: Carbon emissions from land use and land-cover change, *Biogeosciences*, 9, 5125-5142, doi:10.5194/Bg-9-5125-2012, 2012.

Xu Yue 6/24/15 3:34 PM

Formatted: EndNote Bibliography, Left

Xu Yue 6/24/15 3:34 PM

Formatted: EndNote Bibliography, Left

- Knorr, W.: Annual and interannual CO₂ exchanges of the terrestrial biosphere: process-based simulations and uncertainties, *Global Ecol Biogeogr*, 9, 225-252, doi:10.1046/J.1365-2699.2000.00159.X, 2000.
- Koch, D., Bauer, S. E., Del Genio, A., Faluvegi, G., McConnell, J. R., Menon, S., Miller, R. L., Rind, D., Ruedy, R., Schmidt, G. A., and Shindell, D.: Coupled Aerosol-Chemistry-Climate Twentieth-Century Transient Model Investigation: Trends in Short-Lived Species and Climate Responses, *J Climate*, 24, 2693-2714, doi:10.1175/2011jcli3582.1, 2011.
- Koven, C. D., Riley, W. J., Subin, Z. M., Tang, J. Y., Torn, M. S., Collins, W. D., Bonan, G. B., Lawrence, D. M., and Swenson, S. C.: The effect of vertically resolved soil biogeochemistry and alternate soil C and N models on C dynamics of CLM4, *Biogeosciences*, 10, 7109-7131, doi:10.5194/Bg-10-7109-2013, 2013.
- Lamarque, J. F., Shindell, D. T., Josse, B., Young, P. J., Cionni, I., Eyring, V., Bergmann, D., Cameron-Smith, P., Collins, W. J., Doherty, R., Dalsoren, S., Faluvegi, G., Folberth, G., Ghan, S. J., Horowitz, L. W., Lee, Y. H., MacKenzie, I. A., Nagashima, T., Naik, V., Plummer, D., Righi, M., Rumbold, S. T., Schulz, M., Skeie, R. B., Stevenson, D. S., Strode, S., Sudo, K., Szopa, S., Voulgarakis, A., and Zeng, G.: The Atmospheric Chemistry and Climate Model Intercomparison Project (ACCMIP): overview and description of models, simulations and climate diagnostics, *Geosci Model Dev*, 6, 179-206, doi:10.5194/Gmd-6-179-2013, 2013.
- Lathiere, J., Hauglustaine, D. A., Friend, A. D., De Noblet-Ducoudre, N., Viovy, N., and Folberth, G. A.: Impact of climate variability and land use changes on global biogenic volatile organic compound emissions, *Atmos Chem Phys*, 6, 2129-2146, doi:10.5194/acp-6-2129-2006, 2006.
- Liu, H., Tian, F., Hu, H. C., Hu, H. P., and Sivapalan, M.: Soil moisture controls on patterns of grass green-up in Inner Mongolia: an index based approach, *Hydrol Earth Syst Sc*, 17, 805-815, doi:10.5194/Hess-17-805-2013, 2013.
- Lombardozzi, D., Sparks, J. P., and Bonan, G.: Integrating O₃ influences on terrestrial processes: photosynthetic and stomatal response data available for regional and global modeling, *Biogeosciences*, 10, 6815-6831, doi:10.5194/bg-10-6815-2013, 2013.
- Luyssaert, S. and co-authors: CO₂ balance of boreal, temperate, and tropical forests derived from a global database, *Global Change Biol*, 13, 2509-2537, doi:10.1111/J.1365-2486.2007.01439.X, 2007.
- Mahowald, N.: Aerosol Indirect Effect on Biogeochemical Cycles and Climate, *Science*, 334, 794-796, doi:10.1126/Science.1207374, 2011.
- Medlyn, B. E., Duursma, R. A., Eamus, D., Ellsworth, D. S., Prentice, I. C., Barton, C. V. M., Crous, K. Y., de Angelis, P., Freeman, M., and Wingate, L.: Reconciling the optimal and empirical approaches to modelling stomatal conductance, *Global Change Biol*, 17, 2134-2144, doi:10.1111/J.1365-2486.2010.02375.X, 2011.
- Meinshausen, M., Smith, S. J., Calvin, K., Daniel, J. S., Kainuma, M. L. T., Lamarque, J. F., Matsumoto, K., Montzka, S. A., Raper, S. C. B., Riahi, K., Thomson, A., Velders, G. J. M., and van Vuuren, D. P. P.: The RCP greenhouse gas concentrations and their extensions from 1765 to 2300, *Climatic Change*, 109, 213-241, doi:10.1007/S10584-011-0156-Z, 2011.

Xu Yue 6/24/15 3:34 PM

Formatted: EndNote Bibliography, Left

Xu Yue 6/24/15 3:34 PM

Formatted: EndNote Bibliography, Left

Xu Yue 6/24/15 3:34 PM

Formatted: EndNote Bibliography, Left

- 1146 | Mercado, L. M., Bellouin, N., Sitch, S., Boucher, O., Huntingford, C., Wild, M., and
 1147 | Cox, P. M.: Impact of changes in diffuse radiation on the global land carbon sink,
 1148 | *Nature*, 458, 1014-1017, doi:10.1038/Nature07949, 2009.
- 1149 | Miller, R. L. and co-authors: CMIP5 historical simulations (1850-2012) with GISS
 1150 | ModelE2, *J Adv Model Earth Sy*, 6, 441-477, doi:10.1002/2013ms000266, 2014.
- 1151 | Moorcroft, P. R., Hurtt, G. C., and Pacala, S. W.: A method for scaling vegetation
 1152 | dynamics: The ecosystem demography model (ED), *Ecol Monogr*, 71, 557-585,
 1153 | doi:10.1890/0012-9615(2001)071[0557:Amfsvd]2.0.Co;2, 2001.
- 1154 | Murray, M. B., Cannell, M. G. R., and Smith, R. I.: Date of Budburst of fifteen Tree
 1155 | Species in Britain Following Climatic Warming, *J Appl Ecol*, 26, 693-700,
 1156 | doi:10.2307/2404093, 1989.
- 1157 | O'Keefe, J.: Phenology of Woody Species at Harvard Forest since 1990. Harvard Forest
 1158 | Data Archive: HF003., 2000.
- 1159 | Oleson, K. W., Lawrence, D. M., Bonan, G. B., Flanne, M. G., Kluzek, E., Lawrence, P.
 1160 | J., Levis, S., Swenson, S. C., and Thornton, P. E.: Technical Description of version
 1161 | 4.0 of the Community Land Model (CLM), National Center for Atmospheric
 1162 | Research, Boulder, CONCAR/TN-478+STR, 2010.
- 1163 | Olson, D. M., Dinerstein, E., Wikramanayake, E. D., Burgess, N. D., Powell, G. V. N.,
 1164 | Underwood, E. C., D'amico, J. A., Itoua, I., Strand, H. E., Morrison, J. C., Loucks, C.
 1165 | J., Allnutt, T. F., Ricketts, T. H., Kura, Y., Lamoreux, J. F., Wettengel, W. W.,
 1166 | Hedao, P., and Kassem, K. R.: Terrestrial Ecoregions of the World: A New Map of
 1167 | Life on Earth, *Bioscience*, 51, 933-938, doi:10.1641/0006-
 1168 | 3568(2001)051[0933:TEOTWA]2.0.CO;2, 2001.
- 1169 | Pechony, O. and Shindell, D. T.: Fire parameterization on a global scale, *J. Geophys.*
 1170 | *Res.*, 114, D16115, doi:10.1029/2009jd011927, 2009.
- 1171 | Piao, S. L., Sitch, S., Ciais, P., Friedlingstein, P., Peylin, P., Wang, X. H., Ahlstrom, A.,
 1172 | Anav, A., Canadell, J. G., Cong, N., Huntingford, C., Jung, M., Levis, S., Levy, P. E.,
 1173 | Li, J. S., Lin, X., Lomas, M. R., Lu, M., Luo, Y. Q., Ma, Y. C., Myneni, R. B.,
 1174 | Poulter, B., Sun, Z. Z., Wang, T., Viovy, N., Zaehle, S., and Zeng, N.: Evaluation of
 1175 | terrestrial carbon cycle models for their response to climate variability and to CO2
 1176 | trends, *Global Change Biol*, 19, 2117-2132, doi:10.1111/Gcb.12187, 2013.
- 1177 | Pieruschka, R., Huber, G., and Berry, J. A.: Control of transpiration by radiation, *P Natl*
 1178 | *Acad Sci USA*, 107, 13372-13377, doi:10.1073/Pnas.0913177107, 2010.
- 1179 | Porporato, A., Laio, F., Ridolfi, L., and Rodriguez-Iturbe, I.: Plants in water-controlled
 1180 | ecosystems: active role in hydrologic processes and response to water stress - III.
 1181 | Vegetation water stress, *Adv Water Resour*, 24, 725-744, doi:10.1016/S0309-
 1182 | 1708(01)00006-9, 2001.
- 1183 | Potter, C. S., Randerson, J. T., Field, C. B., Matson, P. A., Vitousek, P. M., Mooney, H.
 1184 | A., and Klooster, S. A.: Terrestrial Ecosystem Production - a Process Model-Based
 1185 | on Global Satellite and Surface Data, *Global Biogeochem Cy*, 7, 811-841,
 1186 | doi:10.1029/93gb02725, 1993.
- 1187 | Rayner, N. A., Brohan, P., Parker, D. E., Folland, C. K., Kennedy, J. J., Vanicek, M.,
 1188 | Ansell, T. J., and Tett, S. F. B.: Improved analyses of changes and uncertainties in sea
 1189 | surface temperature measured in situ since the mid-nineteenth century: The HadSST2
 1190 | dataset, *J Climate*, 19, 446-469, doi:10.1175/Jcli3637.1, 2006.

Xu Yue 6/24/15 3:34 PM

Deleted: U1087

Xu Yue 6/24/15 3:34 PM

Deleted: Miller, R. L., Schmidt, G. A., Nazarenko, L. S., Tausnev, N., Bauer, S. E., DelGenio, A. D., Kelley, M., Lo, K. K., Ruedy, R., Shindell, D. T., Aleinov, I., Bauer, M., Bleck, R., Canuto, V., Chen, Y. H., Cheng, Y., Clune, T. L., Faluvegi, G., Hansen, J. E., Healy, R. J., Kiang, N. Y., Koch, D., Lacis, A. A., LeGrande, A. N., Lerner, J., Menon, S., Oinas, V., Garcia-Pando, C. P., Perlwitz, J. P., Puma, M. J., Rind, D., Romanou, A., Russell, G. L., Sato, M., Sun, S., Tsigaridis, K., Unger, N., Voulgarakis, A., Yao, M. S., and Zhang, J. L.:

Xu Yue 6/24/15 3:34 PM

Formatted: EndNote Bibliography, Left

Xu Yue 6/24/15 3:34 PM

Formatted: EndNote Bibliography, Left

- 1205 | Richardson, A. D., Bailey, A. S., Denny, E. G., Martin, C. W., and O'Keefe, J.:
1206 Phenology of a northern hardwood forest canopy, *Global Change Biol*, 12, 1174-
1207 1188, doi:10.1111/j.1365-2486.2006.01164.x, 2006.
- 1208 | Richardson, A. D., Keenan, T. F., Migliavacca, M., Ryu, Y., Sonnentag, O., and Toomey,
1209 M.: Climate change, phenology, and phenological control of vegetation feedbacks to
1210 the climate system, *Agr Forest Meteorol*, 169, 156-173, 2013.
- 1211 | Rienecker, M. M., Suarez, M. J., Gelaro, R., Todling, R., Bacmeister, J., Liu, E.,
1212 Bosilovich, M. G., Schubert, S. D., Takacs, L., Kim, G. K., Bloom, S., Chen, J. Y.,
1213 Collins, D., Conaty, A., Da Silva, A., Gu, W., Joiner, J., Koster, R. D., Lucchesi, R.,
1214 Molod, A., Owens, T., Pawson, S., Pegion, P., Redder, C. R., Reichle, R., Robertson,
1215 F. R., Ruddick, A. G., Sienkiewicz, M., and Woollen, J.: MERRA: NASA's Modern-
1216 Era Retrospective Analysis for Research and Applications, *J Climate*, 24, 3624-3648,
1217 doi:10.1175/Jcli-D-11-00015.1, 2011.
- 1218 | Rosenzweig, C. and Abramopoulos, F.: Land-surface model development for the GISS
1219 GCM, *J Climate*, 10, 2040-2054, doi:10.1175/1520-
1220 0442(1997)010<2040:Lsmdft>2.0.Co;2, 1997.
- 1221 | Sacks, W. J., Deryng, D., Foley, J. A., and Ramankutty, N.: Crop planting dates: an
1222 analysis of global patterns, *Global Ecol Biogeogr*, 19, 607-620, doi:10.1111/J.1466-
1223 8238.2010.00551.X, 2010.
- 1224 | Schaefer, K., Collatz, G. J., Tans, P., Denning, A. S., Baker, I., Berry, J., Prihodko, L.,
1225 Suits, N., and Philpott, A.: Combined Simple Biosphere/Carnegie-Ames-Stanford
1226 Approach terrestrial carbon cycle model, *J. Geophys. Res.*, 113, G03034,
1227 doi:10.1029/2007jg000603, 2008.
- 1228 | Schaefer, K. and co-authors: A model-data comparison of gross primary productivity:
1229 Results from the North American Carbon Program site synthesis, *J. Geophys. Res.*,
1230 117, G03010, doi:10.1029/2012jg001960, 2012.
- 1231 | Schmidt, G. A. and co-authors: Configuration and assessment of the GISS ModelE2
1232 contributions to the CMIP5 archive, *J Adv Model Earth Sy*, 6, 141-184,
1233 doi:10.1002/2013ms000265, 2014.
- 1234 | Schmidt, G. A., Ruedy, R., Hansen, J. E., Aleinov, I., Bell, N., Bauer, M., Bauer, S.,
1235 Cairns, B., Canuto, V., Cheng, Y., Del Genio, A., Faluvegi, G., Friend, A. D., Hall, T.
1236 M., Hu, Y. Y., Kelley, M., Kiang, N. Y., Koch, D., Lacis, A. A., Lerner, J., Lo, K. K.,
1237 Miller, R. L., Nazarenko, L., Oinas, V., Perlwitz, J., Perlwitz, J., Rind, D., Romanou,
1238 A., Russell, G. L., Sato, M., Shindell, D. T., Stone, P. H., Sun, S., Tausnev, N.,
1239 Thresher, D., and Yao, M. S.: Present-day atmospheric simulations using GISS
1240 ModelE: Comparison to in situ, satellite, and reanalysis data, *J Climate*, 19, 153-192,
1241 doi:10.1175/Jcli3612.1, 2006.
- 1242 | Schuster, C., Estrella, N., and Menzel, A.: Shifting and extension of phenological periods
1243 with increasing temperature along elevational transects in southern Bavaria, *Plant*
1244 *Biology*, 16, 332-344, doi:10.1111/Plb.12071, 2014.
- 1245 | Scott, C. E., Rap, A., Spracklen, D. V., Forster, P. M., Carslaw, K. S., Mann, G. W.,
1246 Pringle, K. J., Kivekas, N., Kulmala, M., Lihavainen, H., and Tunved, P.: The direct
1247 and indirect radiative effects of biogenic secondary organic aerosol, *Atmos Chem*
1248 *Phys*, 14, 447-470, doi:10.5194/Acp-14-447-2014, 2014.
- 1249 | Shindell, D. T., Lamarque, J. F., Schulz, M., Flanner, M., Jiao, C., Chin, M., Young, P. J.,
1250 Lee, Y. H., Rotstayn, L., Mahowald, N., Milly, G., Faluvegi, G., Balkanski, Y.,

Xu Yue 6/24/15 3:34 PM

Deleted: , Schwalm, C. R., Williams, C., Arain, M. A., Barr, A., Chen, J. M., Davis, K. J., Dimitrov, D., Hilton, T. W., Hollinger, D. Y., Humphreys, E., Poulter, B., Raczka, B. M., Richardson, A. D., Sahoo, A., Thornton, P., Vargas, R., Verbeeck, H., Anderson, R., Baker, I., Black, T. A., Bolstad, P., Chen, J. Q., Curtis, P. S., Desai, A. R., Dietze, M., Dragoni, D., Gough, C., Grant, R. F., Gu, L. H., Jain, A., Kucharik, C., Law, B., Liu, S. G., Lokipitiya, E., Margolis, H. A., Matamala, R., McCaughey, J. H., Monson, R., Munger, J. W., Oechel, W., Peng, C. H., Price, D. T., Ricciuto, D., Riley, W. J., Roulet, N., Tian, H. Q., Tonitto, C., Torn, M., Weng, E. S., and Zhou, X. L.:

Xu Yue 6/24/15 3:34 PM

Deleted: , Kelley, M., Nazarenko, L., Ruedy, R., Russell, G. L., Aleinov, I., Bauer, M., Bauer, S. E., Bhat, M. K., Bleck, R., Canuto, V., Chen, Y. H., Cheng, Y., Clune, T. L., Del Genio, A., de Fainchtein, R., Faluvegi, G., Hansen, J. E., Healy, R. J., Kiang, N. Y., Koch, D., Lacis, A. A., LeGrande, A. N., Lerner, J., Lo, K. K., Matthews, E. E., Menon, S., Miller, R. L., Oinas, V., Olosio, A. O., Perlwitz, J. P., Puma, M. J., Putman, W. M., Rind, D., Romanou, A., Sato, M., Shindell, D. T., Sun, S., Syed, R. A., Tausnev, N., Tsigaridis, K., Unger, N., Voulgarakis, A., Yao, M. S., and Zhang, J. L.:

1281 [Collins, W. J., Conley, A. J., Dalsoren, S., Easter, R., Ghan, S., Horowitz, L., Liu, X.,](#)
1282 [Myhre, G., Nagashima, T., Naik, V., Rumbold, S. T., Skeie, R., Sudo, K., Szopa, S.,](#)
1283 [Takemura, T., Voulgarakis, A., Yoon, J. H., and Lo, F.: Radiative forcing in the](#)
1284 [ACCMIP historical and future climate simulations, *Atmos Chem Phys*, 13, 2939-](#)
1285 [2974, doi:10.5194/Acp-13-2939-2013, 2013a.](#)
1286 [Shindell, D. T., Pechony, O., Voulgarakis, A., Faluvegi, G., Nazarenko, L., Lamarque, J.](#)
1287 [F., Bowman, K., Milly, G., Kovari, B., Ruedy, R., and Schmidt, G. A.: Interactive](#)
1288 [ozone and methane chemistry in GISS-E2 historical and future climate simulations,](#)
1289 [Atmos Chem Phys, 13, 2653-2689, doi:10.5194/Acp-13-2653-2013, 2013b.](#)
1290 Simard, M., Pinto, N., Fisher, J. B., and Baccini, A.: Mapping forest canopy height
1291 globally with spaceborne lidar, *J. Geophys. Res.*, 116, G04021,
1292 doi:10.1029/2011jg001708, 2011.
1293 Sitch, S., Cox, P. M., Collins, W. J., and Huntingford, C.: Indirect radiative forcing of
1294 climate change through ozone effects on the land-carbon sink, *Nature*, 448, 791-794,
1295 doi:10.1038/Nature06059, 2007.
1296 Sitch, S., Friedlingstein, P., Gruber, N., Jones, S. D., Murray-Tortarolo, G., Ahlström, A.,
1297 Doney, S. C., Graven, H., Heinze, C., Huntingford, C., Levis, S., Levy, P. E., Lomas,
1298 M., Poulter, B., Viovy, N., Zaehle, S., Zeng, N., Arneth, A., Bonan, G., Bopp, L.,
1299 Canadell, J. G., Chevallier, F., Ciais, P., Ellis, R., Gloor, M., Peylin, P., Piao, S. L.,
1300 Quéré, C. L., Smith, B., Zhu, Z., and Myneni, R.: Recent trends and drivers of
1301 regional sources and sinks of carbon dioxide, *Biogeosciences*, 12, 653-679, 2015.
1302 Sitch, S., Smith, B., Prentice, I. C., Arneth, A., Bondeau, A., Cramer, W., Kaplan, J. O.,
1303 Levis, S., Lucht, W., Sykes, M. T., Thonicke, K., and Venevsky, S.: Evaluation of
1304 ecosystem dynamics, plant geography and terrestrial carbon cycling in the LPJ
1305 dynamic global vegetation model, *Global Change Biol*, 9, 161-185,
1306 doi:10.1046/J.1365-2486.2003.00569.X, 2003.
1307 Spitters, C. J. T., Toussaint, H. A. J. M., and Goudriaan, J.: Separating the Diffuse and
1308 Direct Component of Global Radiation and Its Implications for Modeling Canopy
1309 Photosynthesis [1. Components of Incoming Radiation](#), *Agr Forest Meteorol*, 38, 217-
1310 229, doi:10.1016/0168-1923(86)90060-2, 1986.
1311 [Stephenson, N. L. and van Mantgem, P. J.: Forest turnover rates follow global and](#)
1312 [regional patterns of productivity, *Ecol Lett*, 8, 524-531, doi:10.1111/J.1461-](#)
1313 [0248.2005.00746.X, 2005.](#)
1314 Sugiura, D. and Tateno, M.: Optimal Leaf-to-Root Ratio and Leaf Nitrogen Content
1315 Determined by Light and Nitrogen Availabilities, *Plos One*, 6, e22236,
1316 doi:10.1371/journal.pone.0022236, 2011.
1317 [Thomas, R. Q., Zaehle, S., Templer, P. H., and Goodale, C. L.: Global patterns of](#)
1318 [nitrogen limitation: confronting two global biogeochemical models with observations,](#)
1319 [Global Change Biol, 19, 2986-2998, doi:10.1111/Gcb.12281, 2013.](#)
1320 Thornton, P. E., Lamarque, J. F., Rosenbloom, N. A., and Mahowald, N. M.: Influence of
1321 carbon-nitrogen cycle coupling on land model response to CO2 fertilization and
1322 climate variability, *Global Biogeochem Cy*, 21, Gb4018, doi:10.1029/2006gb002868,
1323 2007.
1324 Unger, N.: Global climate impact of civil aviation for standard and desulfurized jet fuel,
1325 *Geophys. Res. Lett.*, 38, L20803, doi:10.1029/2011gl049289, 2011.

Xu Yue 6/24/15 3:34 PM

Formatted: EndNote Bibliography, Left

Xu Yue 6/24/15 3:34 PM

Deleted: 2013

Xu Yue 6/24/15 3:34 PM

Deleted: 2. Calculation

Xu Yue 6/24/15 3:34 PM

Deleted: Canopy Photosynthesis

Xu Yue 6/24/15 3:34 PM

Deleted: 231-242

Xu Yue 6/24/15 3:34 PM

Deleted: 90061-4

Xu Yue 6/24/15 3:34 PM

Formatted: EndNote Bibliography, Left

Xu Yue 6/24/15 3:34 PM

Formatted: EndNote Bibliography, Left

- 1331 | Unger, N.: Human land-use-driven reduction of forest volatiles cools global climate, *Nat*
 1332 | *Clim Change*, 4, 907-910, doi:10.1038/Nclimate2347, 2014a.
- 1333 | Unger, N.: Isoprene emission variability through the twentieth century, *J. Geophys. Res.*,
 1334 | 118, 13606-13613, doi:10.1002/2013jd020978, 2013.
- 1335 | Unger, N.: On the role of plant volatiles in anthropogenic global climate change,
 1336 | *Geophys Res Lett*, 41, 8563-8569, doi:10.1002/2014gl061616, 2014b.
- 1337 | Unger, N., Harper, K., Zheng, Y., Kiang, N. Y., Aleinov, I., Arneth, A., Schurgers, G.,
 1338 | Amelynck, C., Goldstein, A., Guenther, A., Heinesch, B., Hewitt, C. N., Karl, T.,
 1339 | Laffineur, Q., Langford, B., McKinney, K. A., Misztal, P., Potosnak, M., Rinne, J.,
 1340 | Pressley, S., Schoon, N., and Serça, D.: Photosynthesis-dependent isoprene emission
 1341 | from leaf to planet in a global carbon–chemistry–climate model, *Atmos. Chem. Phys.*,
 1342 | 13, 17717-17791, doi:10.5194/acp-13-10243-2013, 2013.
- 1343 | Unger, N. and Yue, X.: Strong chemistry- climate feedbacks in the Pliocene, *Geophys.*
 1344 | *Res. Lett.*, 41, 527-533, doi:10.1002/2013gl058773, 2014.
- 1345 | Val Martin, M., Heald, C. L., and Arnold, S. R.: Coupling dry deposition to vegetation
 1346 | phenology in the Community Earth System Model: Implications 3 for the simulation
 1347 | of surface O₃, *Geophys. Res. Lett.*, 8, 2988-2996, doi:10.1002/2014GL059651, 2014.
- 1348 | Vitasse, Y., Delzon, S., Dufrene, E., Pontailier, J. Y., Louvet, J. M., Kremer, A., and
 1349 | Michalet, R.: Leaf phenology sensitivity to temperature in European trees: Do within-
 1350 | species populations exhibit similar responses?, *Agr Forest Meteorol*, 149, 735-744,
 1351 | doi:10.1016/J.Agrformet.2008.10.019, 2009.
- 1352 | von Caemmerer, S. and Farquhar, G. D.: Some Relationships between the Biochemistry
 1353 | of Photosynthesis and the Gas-Exchange of Leaves, *Planta*, 153, 376-387, 1981.
- 1354 | Weedon, G. P., Balsamo, G., Bellouin, N., Gomes, S., Best, M. J., and Viterbo, P.: The
 1355 | WFDEI meteorological forcing data set: WATCH Forcing Data methodology applied
 1356 | to ERA-Interim reanalysis data, *Water Resources Research*, 50, 7505-7514,
 1357 | doi:10.1002/2014wr015638, 2014.
- 1358 | White, M. A., Thornton, P. E., and Running, S. W.: A continental phenology model for
 1359 | monitoring vegetation responses to interannual climatic variability, *Global*
 1360 | *Biogeochem Cy*, 11, 217-234, doi:10.1029/97gb00330, 1997.
- 1361 | Wittig, V. E., Ainsworth, E. A., and Long, S. P.: To what extent do current and projected
 1362 | increases in surface ozone affect photosynthesis and stomatal conductance of trees? A
 1363 | meta-analytic review of the last 3 decades of experiments, *Plant Cell Environ*, 30,
 1364 | 1150-1162, doi:10.1111/J.1365-3040.2007.01717.X, 2007.
- 1365 | Yienger, J. J. and Levy, H.: Empirical-Model of Global Soil-Biogenic Nox Emissions, *J.*
 1366 | *Geophys. Res.*, 100, 11447-11464, doi:10.1029/95jd00370, 1995.
- 1367 | Yue, X. and Unger, N.: Ozone vegetation damage effects on gross primary productivity
 1368 | in the United States, *Atmos. Chem. Phys.*, 14, 9137-9153, doi:10.5194/acp-14-9137-
 1369 | 2014, 2014.
- 1370 | Yue, X., Unger, N., Keenan, T. F., Zhang, X., and Vogel, C. S.: Probing the past 30-year
 1371 | phenology trend of U.S. deciduous forests, *Biogeosciences Discuss.*, 12, 6037-6080,
 1372 | doi:10.5194/bgd-12-6037-2015, 2015a.
- 1373 | Yue, X., Unger, N., and Zheng, Y.: Distinguishing the drivers of trends in land carbon
 1374 | fluxes and biogenic emissions over the past three decades, *Atmos. Chem. Phys.*,
 1375 | submitted, 2015b.

Xu Yue 6/24/15 3:34 PM

Deleted: Resour Res

Xu Yue 6/24/15 3:34 PM

Deleted: submitted

Xu Yue 6/24/15 3:34 PM

Deleted: in preparation

1379 | Zaehle, S., Medlyn, B. E., De Kauwe, M. G., Walker, A. P., Dietze, M. C., Hickler, T.,
1380 | Luo, Y. Q., Wang, Y. P., El-Masri, B., Thornton, P., Jain, A., Wang, S. S., Warland,
1381 | D., Weng, E. S., Parton, W., Iversen, C. M., Gallet-Budynek, A., McCarthy, H.,
1382 | Finzi, A. C., Hanson, P. J., Prentice, I. C., Oren, R., and Norby, R. J.: Evaluation of
1383 | 11 terrestrial carbon-nitrogen cycle models against observations from two temperate
1384 | Free-Air CO₂ Enrichment studies, *New Phytol*, 202, 803-822,
1385 | doi:10.1111/Nph.12697, 2014.

1386 | Zeng, N., Mariotti, A., and Wetzel, P.: Terrestrial mechanisms of interannual CO₂
1387 | variability, *Global Biogeochem Cy*, 19, Gb1016, doi:10.1029/2004gb0022763, 2005.

1388 | Zhang, X. Y., Tan, B., and Yu, Y. Y.: Interannual variations and trends in global land
1389 | surface phenology derived from enhanced vegetation index during 1982-2010, *Int J*
1390 | *Biometeorol*, 58, 547-564, doi:10.1007/S00484-014-0802-Z, 2014.

1391 | Zhao, M. S., Heinsch, F. A., Nemani, R. R., and Running, S. W.: Improvements of the
1392 | MODIS terrestrial gross and net primary production global data set, *Remote Sens*
1393 | *Environ*, 95, 164-176, doi:10.1016/J.Rse.2004.12.011, 2005.

1394 | Zhao, M. S. and Running, S. W.: Drought-Induced Reduction in Global Terrestrial Net
1395 | Primary Production from 2000 Through 2009, *Science*, 329, 940-943,
1396 | doi:10.1126/Science.1192666, 2010.

1397 | Zheng, Y., Unger, N., Barley, M., and Yue, X.: Relationships between photosynthesis
1398 | and formaldehyde as a probe of isoprene emission, *Atmos. Chem. Phys. Discuss.*, 15,
1399 | 11763-11797, 2015.

1400 | Zhu, Z. C., Bi, J., Pan, Y. Z., Ganguly, S., Anav, A., Xu, L., Samanta, A., Piao, S. L.,
1401 | Nemani, R. R., and Myneni, R. B.: Global Data Sets of Vegetation Leaf Area Index
1402 | (LAI)3g and Fraction of Photosynthetically Active Radiation (FPAR)3g Derived
1403 | from Global Inventory Modeling and Mapping Studies (GIMMS) Normalized
1404 | Difference Vegetation Index (NDVI3g) for the Period 1981 to 2011, *Remote Sens*, 5,
1405 | 927-948, doi:10.3390/Rs5020927, 2013.

1406 |

1407 |

1408 |

Xu Yue 6/24/15 3:34 PM

Deleted: CO(2)

Xu Yue 6/24/15 3:34 PM

Deleted: submitted

Xu Yue 6/24/15 3:34 PM

Deleted: -Basel

Xu Yue 6/24/15 3:34 PM

Deleted: -

Xu Yue 6/24/15 3:34 PM

Deleted: Page Break

... [2]

1416 **Table 1.** Photosynthetic and allometric parameters for the vegetation model.
1417

PFT ^a	TDA	GRAC3	GRAC4	SHR	DBF	ENF	EBF	CROC3	CROC4
Carboxylation	C3	C3	C4	C3	C3	C3	C3	C3	C4
V_{max}^{25} ($\mu\text{mol m}^{-2} \text{s}^{-1}$)	33	43	24	38	45	43	40	40	40
m	9	9	5	9	9	9	9	11	5
b ($\text{mmol m}^{-2} \text{s}^{-1}$)	2	2	2	2	2	2	2	8	2
a_{wl} (kg C m^{-2})	0.1	0.005	0.005	0.1	0.95	0.85	0.95	0.005	0.005
b_{wl}	1.667	1.667	1.667	1.667	1.667	1.667	1.667	1.667	1.667
σ_l (kg C m^{-2} LAI^{-1})	0.05	0.025	0.05	0.05	0.0375	0.1	0.0375	0.025	0.05
η (kg C m^{-1} LAI^{-1})	0.01	0.01	0.01	0.01	0.01	0.01	0.01	0.01	0.01
n_0 ($\text{kg N} [\text{kg C}]^{-1}$)	0.06	0.073	0.06	0.06	0.046	0.033	0.046	0.073	0.06
n_{rl}	0.5	1	1	0.5	0.5	0.75	0.5	1	1
n_{wl}	0.1	1	1	0.1	0.1	0.1	0.1	1	1
r_g	0.2	0.2	0.2	0.2	0.2	0.2	0.2	0.2	0.2
LAI_{min}	1	1	1	1	1	1	1	1	1
LAI_{max}	3	3	3	3	9	5	9	3	3
γ_r (360 days) ⁻¹	0.5	0.75	0.75	0.5	0.75	0.25	0.75	0.75	0.75
γ_w (360 days) ⁻¹	0.1	0.2	0.2	0.1	0.015	0.01	0.015	0.2	0.2
H_0 (m)	1	0.8	1.3	1	19	16.5	19	0.8	1.3

1418

1419 ^a Plant functional types (PFTs) are tundra (TDA), C3 grassland (GRAC3), C4
1420 savanna/grassland (GRAC4), shrubland (SHR), deciduous broadleaf forest (DBF),
1421 evergreen needleleaf forest (ENF), evergreen broadleaf forest (EBF), and C3/C4 cropland
1422 (CROC3/CROC4).

1423 |

Xu Yue 6/24/15 3:34 PM

Deleted: .

1425
1426
1427 **Table 2.** Phenological parameters for the vegetation model.
1428

Variables	Description	Units	Value	Reference
T_b	Base temperature for budburst forcing	°C	5	Murray et al. (1989)
a	Parameters for budburst threshold G_b	Degree day	-110	Calibrated (Y2015)
b	Parameters for budburst threshold G_b	Degree day	550	Calibrated (Y2015)
r	Parameters for budburst threshold G_b	Dimensionless	-0.01	Murray et al. (1989)
L_g	Growing length	Degree day	380	Calibrated (Y2015)
T_s	Base temperature for senescence forcing	°C	20	Dufrene et al. (2005)
F_s	Threshold for leaf fall	Degree day	-140	Calibrated (Y2015)
L_f	Falling length	Degree day	410	Calibrated (Y2015)
P_x	Daylength threshold for leaf fall	Minutes	695	White et al. (1997)
P_i	Daylength threshold for full dormancy	Minutes	585	Calibrated (Y2015)
T_d	Threshold for drought phenology	°C	12	Calibrated (Fig. 2)
β_{\min}	Lower threshold of drought limit for shrub	Dimensionless	0.4	Calibrated (Fig. S1)
β_{\max}	Upper threshold of drought limit for shrub	Dimensionless	1	Calibrated (Fig. S1)
ST_b	Base soil temperature for budburst forcing	°C	0	White et al. (1997)
SG_b	Threshold for budburst with soil temperature	Degree day	100	Calibrated
SL_g	Growing length with soil temperature	Degree day	100	Calibrated
ST_s	Base soil temperature for senescence forcing	°C	10	Calibrated
SF_s	Threshold for leaf fall with soil temperature	Degree day	-80	Calibrated
SL_f	Falling length with soil temperature	Degree day	100	Calibrated
β_{\min}	Lower threshold of drought limit for herbs	Dimensionless	0.3	Calibrated (Fig. S1)
β_{\max}	Upper threshold of drought limit for herbs	Dimensionless	0.9	Calibrated (Fig. S1)

1429
1430
1431

1432
1433
1434
1435
1436
1437
1438

Table 3. Summary of carbon fluxes and ozone vegetation damage in different domains and for tropics (23°S-23°N).

Regions	Amazon	North America	Central Africa	Europe	East Asia	Indonesia	Tropics	Global
GPP (Pg C a ⁻¹)	33.4	12.3	25.7	11.5	17.9	6.7	77.9	
NPP (Pg C a ⁻¹)	15.5	7.5	12.1	7.3	10.3	2.9	36.8	
NEE (Pg C a ⁻¹)	-0.4	-0.5	-0.3	-0.4	-0.5	-0.1	-1.0	
Ra (Pg C a ⁻¹)	17.9	4.8	13.6	4.2	7.6	3.8	41.1	
Rh (Pg C a ⁻¹)	15.1	7	11.8	6.9	9.8	2.8	35.8	
Low ozone damage to GPP (%)	-0.9	-2.4	-1.8	-2.5	-4.3	-3	-1.7	
High ozone damage to GPP (%)	-2.6	-5.8	-4.4	-6.1	-9.6	-7.3	-4.4	
Low ozone damage to LAI (%)	-0.3	-0.5	-0.6	-0.5	-0.9	-0.8	-0.5	
High ozone damage to LAI (%)	-0.8	-1.2	-1.6	-1.4	-2.4	-2.1	-1.4	

Xu Yue 6/24/15 3:34 PM

Inserted Cells

Xu Yue 6/24/15 3:34 PM

Formatted: Font:11 pt

Xu Yue 6/24/15 3:34 PM

Formatted Table

Xu Yue 6/24/15 3:34 PM

Formatted: Font:11 pt

Xu Yue 6/24/15 3:34 PM

Formatted: Font:11 pt

Xu Yue 6/24/15 3:34 PM

Formatted: Font:11 pt

Xu Yue 6/24/15 3:34 PM

Formatted: Font:11 pt

Xu Yue 6/24/15 3:34 PM

Formatted: Font:11 pt

Xu Yue 6/24/15 3:34 PM

Formatted: Font:11 pt

Xu Yue 6/24/15 3:34 PM

Inserted Cells

Xu Yue 6/24/15 3:34 PM

Formatted: Font:11 pt

1439
1440
1441
1442
1443

Figure captions

Figure 1. Distribution of 145 sites from the FLUXNET and the North American Carbon Program (NACP) network. The duplicated sites have been removed. The color indicates different plant functional types (PFTs) as evergreen needleleaf forest (ENF, blue), evergreen broadleaf forest (EBF, cyan), deciduous broadleaf forest (DBF, magenta), shrubland (SHR, yellow) grassland (GRA, green), and cropland (CRO, red). “Mixed Forests” are classified as ENF, “Permanent Wetlands”, “Savannas”, and “Woody Savannas” as SHR. The PFT of each site is described in supplemental Table S1.

Figure 2. Correlations between monthly gross primary productivity (GPP) and soil variables at (a, b) shrub and (c, d) grass sites. For each site, we calculate correlation coefficients of GPP-soil temperature (red points) and GPP-soil moisture (blue squares). These correlation coefficients are then plotted against the annual mean (a, c) soil temperature (°C) or (b, d) soil moisture (fraction) at each site.

Figure 3. Comparison between observed and simulated monthly GPP from FLUXNET and NACP networks grouped by PFTs. Each point represents the average value of one month at one site. The red lines indicate linear regression between observations and simulations. The regression fit, correlation coefficient, and relative bias are shown on each panel. The PFTs include evergreen needleleaf forest (ENF), evergreen broadleaf forest (EBF), deciduous broadleaf forest (DBF), shrubland (SHR), grassland (GRA), and cropland (CRO). The detailed comparison for each site is shown in Fig. S2. Units of GPP: $\text{g C m}^{-2} \text{ day}^{-1}$.

Figure 4. Bar charts of (a, d) correlation coefficients (R), (b, e) biases, and (c, f) RMSE for monthly (a, b, c) GPP and (d, e, f) net ecosystem exchange (NEE) between simulations and observations at 145 sites. Each bar represents the number of sites where the R , bias, or RMSE of simulations fall between the specific ranges as defined by the x-axis intervals. The minimum and maximum of each statistical metric are indicated as the two ends of x-axis in the plots. The values of x-axis are not even. The absolute biases

Xu Yue 6/24/15 3:34 PM

Deleted: land

Xu Yue 6/24/15 3:34 PM

Deleted: local vegetation type at

Xu Yue 6/24/15 3:34 PM

Deleted: plant function types (

Xu Yue 6/24/15 3:34 PM

Deleted:).

Xu Yue 6/24/15 3:34 PM

Deleted: land types

Xu Yue 6/24/15 3:34 PM

Deleted: Histogram

Xu Yue 6/24/15 3:34 PM

Deleted: b

Xu Yue 6/24/15 3:34 PM

Deleted: c, d

Xu Yue 6/24/15 3:34 PM

Deleted: e

Xu Yue 6/24/15 3:34 PM

Deleted: , e

Xu Yue 6/24/15 3:34 PM

Deleted: b,

instead of relative biases are shown for NEE because the long-term average NEE (the denominator) is usually close to zero at most sites. The **PFT** definitions are: ENF, Evergreen Needleleaf Forest; EBF, Evergreen Broadleaf Forest; DBF, Deciduous Broadleaf Forest; SHR, Shrubland; GRA, Grasslands; CRO, Croplands. Detailed comparisons at each site are shown in Figs. S2 and S4.

Figure 5. Simulated (a) tree height, (c) leaf area index (LAI), and (e) GPP and their differences relative to observations (b, d, f). GPP dataset is from Jung et al. (2009). Simulations are performed with WFDEI reanalysis. Statistics are the annual average for period 1982-2011. The boxes in (a) represent six regions used for seasonal comparison in Fig. 6.

Figure 6. Comparison of annual (a) tree height and seasonal (b) LAI, (c) GPP, and (d) net primary productivity (NPP) between simulations and observations for the six regions shown in Fig. 5a. GPP dataset is from Jung et al. (2009). Values at different regions are marked using different symbols, with distinct colors indicating seasonal means for winter (blue, December-February), spring (green, March-May), summer (red, June-August), and autumn (magenta, September-November).

Figure 7. Comparison of simulated global GPP and net biome productivity (NBP) from (red) YIBs-offline and (blue) ModelE2-YIBs models with 10 other carbon cycle models for 1982-2008. Each black symbol represents an independent model as summarized in Piao et al. (2013). Error bars indicate the standard deviations for interannual variability. The gray shading represents global residual land sink (RLS) calculated in Friedlingstein et al. (2010). The green line on the top represents range of GPP for 1982-2008 estimated by Jung et al. (2011) and the magenta line represents GPP for 1982-2011 from Jung et al. (2009).

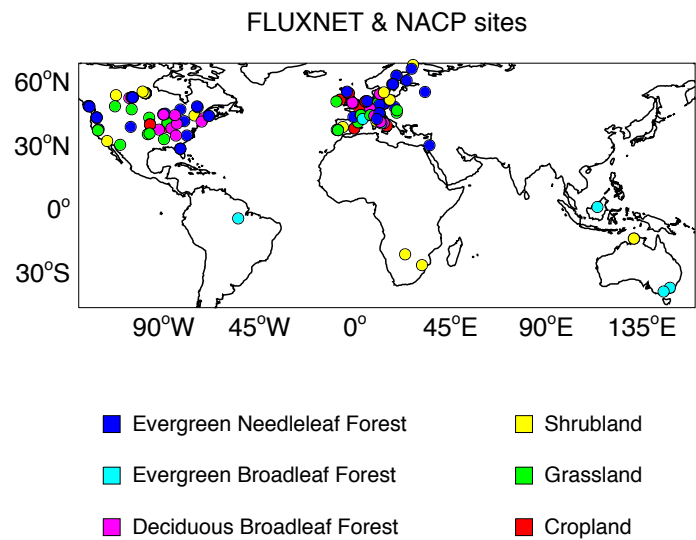
Figure 8. Comparison of simulated budburst dates in Northern Hemisphere with remote sensing. Simulated phenology in each grid square is the composite result from DBF, tundra, shrubland, and grassland based on PFT fraction and LAI in that grid box. Both

Xu Yue 6/24/15 3:34 PM
Deleted: land cover

simulations and observations are averaged for period 1982-2011. Results for Southern Hemisphere are not shown due to the limit coverage of deciduous forests and cold grass species.

Figure 9. Percentage of ozone vegetation damage to (top) GPP and (bottom) LAI with (a, c) low and (b, d) high sensitivity. Both damages of GPP and LAI are averaged for 1982-2011. Offline surface ozone concentrations (Fig. S5) are simulated by GISS ModelE2 with climatology of the year 2000.

1529
1530
1531



1532 **Figure 1.** Distribution of 145 sites from the FLUXNET and the North American Carbon
1533 Program (NACP) network. The duplicated sites have been removed. The color indicates
1534 different plant functional types (PFTs) as evergreen needleleaf forest (ENF, blue),
1535 evergreen broadleaf forest (EBF, cyan), deciduous broadleaf forest (DBF, magenta),
1536 shrublands (SHR, yellow) grasslands (GRA, green), and croplands (CRO, red). “Mixed
1537 Forests” are classified as ENF, “Permanent Wetlands”, “Savannas”, and “Woody
1538 Savannas” as SHR. The PFT of each site is described in supplemental Table S1.
1539
1540

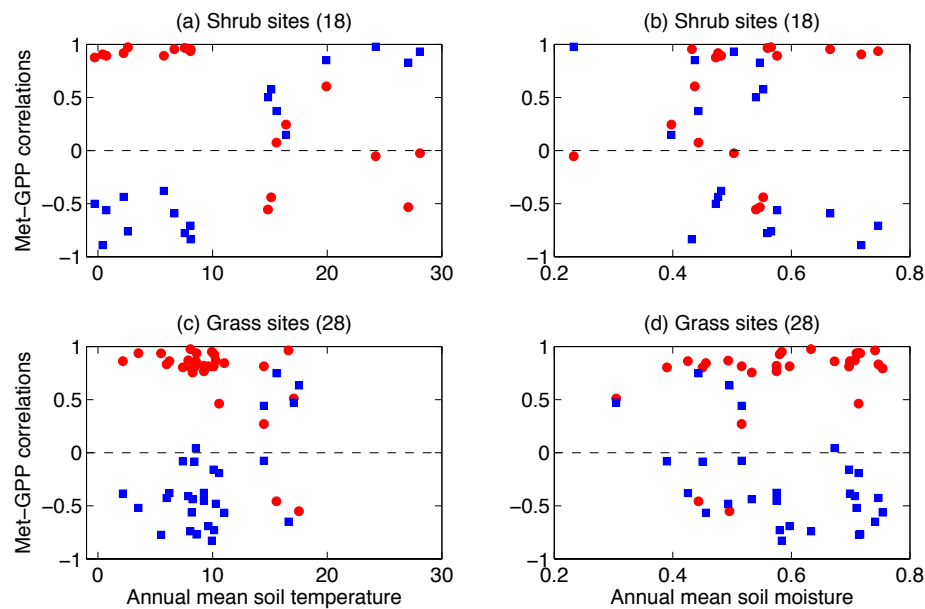


Figure 2. Correlations between monthly gross primary productivity (GPP) and soil variables at (a, b) shrub and (c, d) grass sites. For each site, we calculate correlation coefficients of GPP-soil temperature (red points) and GPP-soil moisture (blue squares). These correlation coefficients are then plotted against the annual mean (a, c) soil temperature (°C) or (b, d) soil moisture (fraction) at each site.

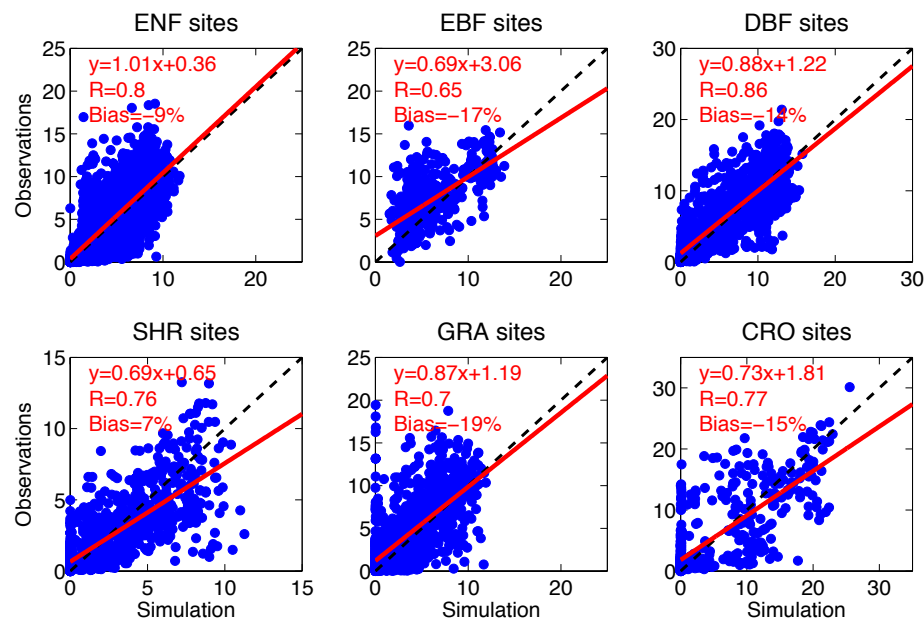
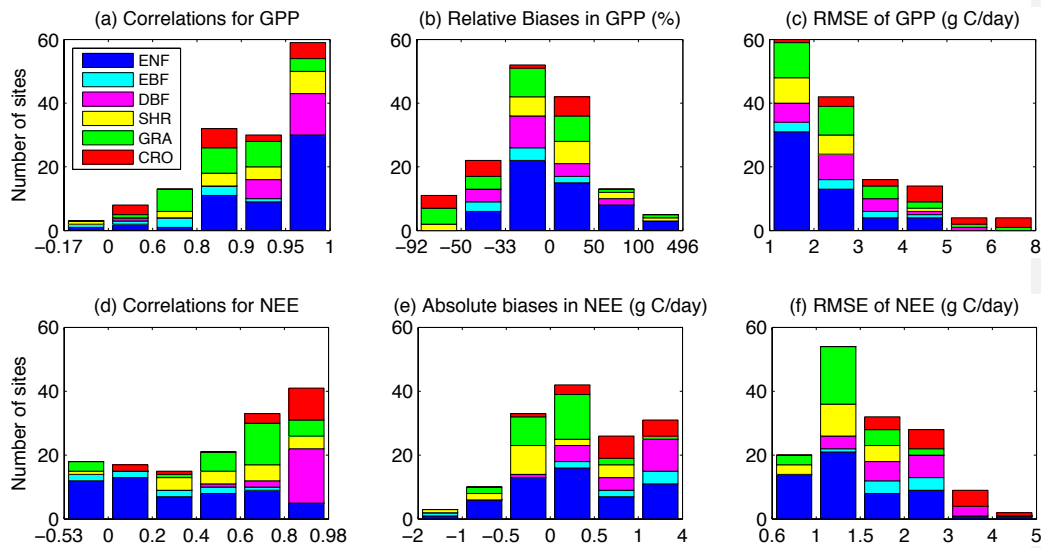


Figure 3. Comparison between observed and simulated monthly GPP from FLUXNET and NACP networks grouped by PFTs. Each point represents the average value of one month at one site. The red lines indicate linear regression between observations and simulations. The regression fit, correlation coefficient, and relative bias are shown on each panel. The PFTs include evergreen needleleaf forest (ENF), evergreen broadleaf forest (EBF), deciduous broadleaf forest (DBF), shrublands (SHR), grasslands (GRA), and croplands (CRO). The detailed comparison for each site is shown in Fig. S2. Units of GPP: $\text{g C m}^{-2} \text{ day}^{-1}$.

1574
1575



1576
1577

1578 **Figure 4.** Bar charts of (a, d) correlation coefficients (R), (b, e) biases, and (c, f) RMSE
 1579 for monthly (a, b, c) GPP and (d, e, f) net ecosystem exchange (NEE) between
 1580 simulations and observations at 145 sites. Each bar represents the number of sites where
 1581 the R , bias, or RMSE of simulations fall between the specific ranges as defined by the x-
 1582 axis intervals. The minimum and maximum of each statistical metric are indicated as the
 1583 two ends of x-axis in the plots. The values of x-axis are not even. The absolute biases
 1584 instead of relative biases are shown for NEE because the long-term average NEE (the
 1585 denominator) is usually close to zero at most sites. The PFT definitions are: ENF,
 1586 Evergreen Needleleaf Forest; EBF, Evergreen Broadleaf Forest; DBF, Deciduous
 1587 Broadleaf Forest; SHR, Shrubland; GRA, Grasslands; CRO, Croplands. Detailed
 1588 comparisons at each site are shown in Figs. S2 and S4.
 1589

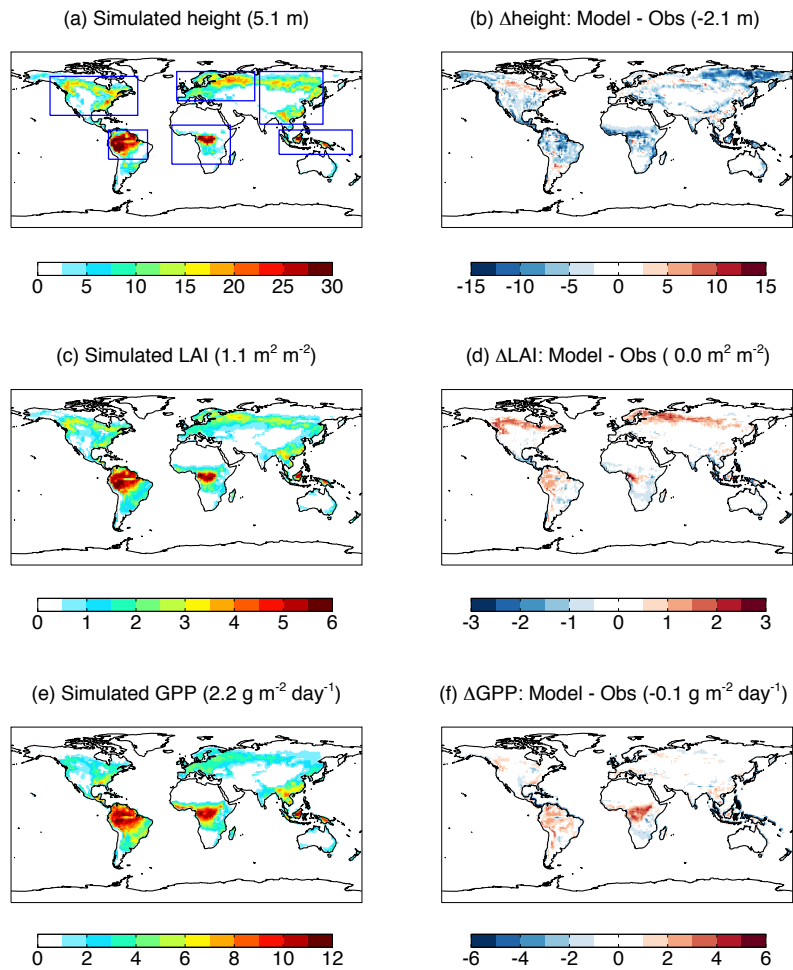
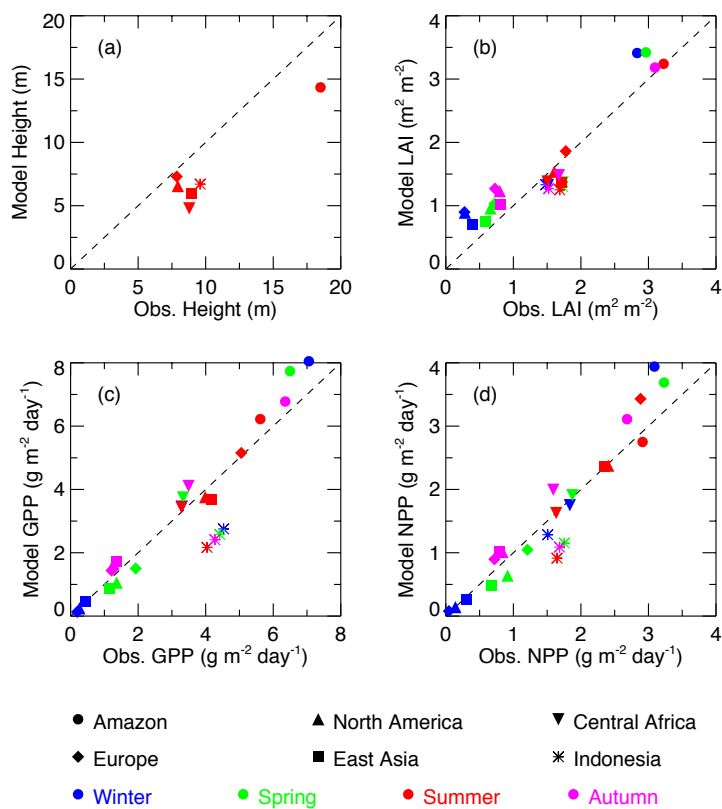


Figure 5. Simulated (a) tree height, (c) leaf area index (LAI), and (e) GPP and their differences relative to observations (b, d, f). GPP dataset is from Jung et al. (2009). Simulations are performed with WFDEI reanalysis. Statistics are the annual average for period 1982-2011. The boxes in (a) represent six regions used for seasonal comparison in Fig. 6.

1598
1599



1600
1601
1602
1603
1604
1605
1606
1607
1608
1609

Figure 6. Comparison of annual (a) tree height and seasonal (b) LAI, (c) GPP, and (d) net primary productivity (NPP) between simulations and observations for the six regions shown in Fig. 5a. GPP dataset is from Jung et al. (2009). Values at different regions are marked using different symbols, with distinct colors indicating seasonal means for winter (blue, December-February), spring (green, March-May), summer (red, June-August), and autumn (magenta, September-November).

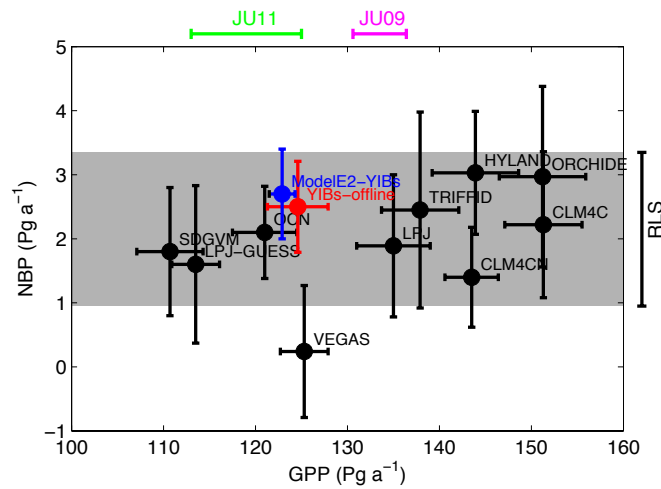


Figure 7. Comparison of simulated global GPP and net biome productivity (NBP) from (red) YIBs-offline and (blue) ModelE2-YIBs models with 10 other carbon cycle models for 1982-2008. Each black symbol represents an independent model as summarized in Piao et al. (2013). Error bars indicate the standard deviations for interannual variability. The gray shading represents global residual land sink (RLS) calculated in Friedlingstein et al. (2010). The green line on the top represents range of GPP for 1982-2008 estimated by Jung et al. (2011) and the magenta line represents GPP for 1982-2011 from Jung et al. (2009).

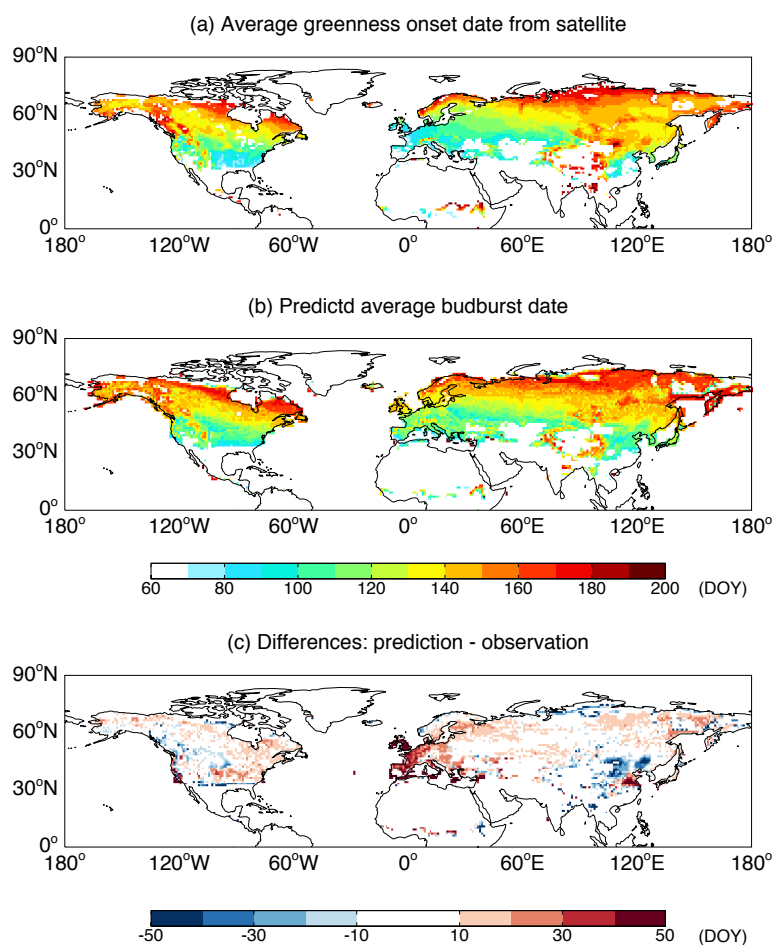
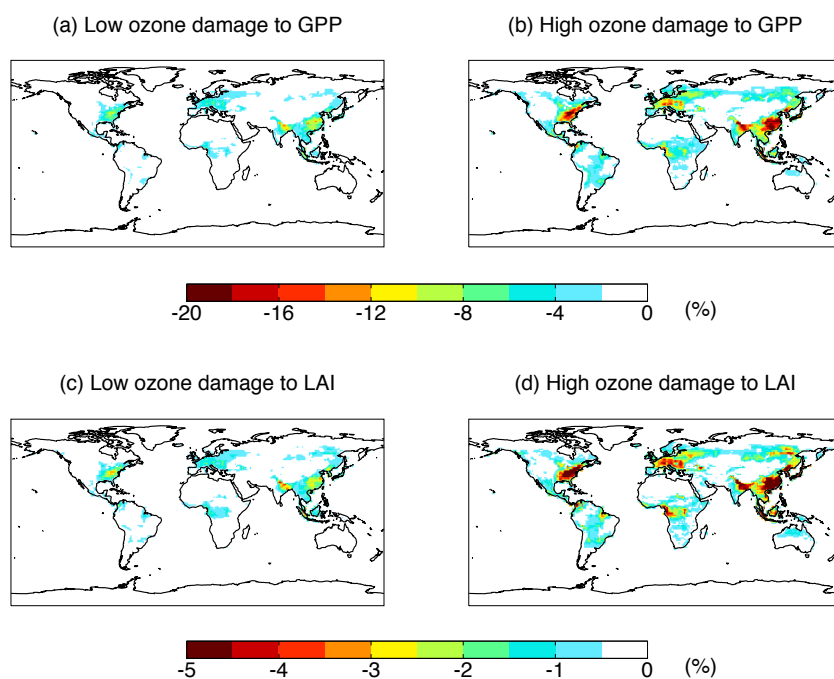


Figure 8. Comparison of simulated budburst dates in Northern Hemisphere with remote sensing. Simulated phenology in each grid square is the composite result from DBF, tundra, shrubland, and grassland based on PFT fraction and LAI in that grid box. Both simulations and observations are averaged for period 1982-2011. Results for Southern Hemisphere are not shown due to the limit coverage of deciduous forests and cold grass species.

1655
1656
1657
1658



1659
1660
1661
1662
1663
1664
1665
1666
1667
1668
1669
1670
1671
1672
1673

Figure 9. Percentage of ozone vegetation damage to (top) GPP and (bottom) LAI with (a, c) low and (b, d) high sensitivity. Both damages of GPP and LAI are averaged for 1982-2011. Offline surface ozone concentrations (Fig. S5) are simulated by GISS ModelE2 with climatology of the year 2000.